GFZ
Helmholtz-Zentrum
POTSDAM

HELMHOLTZ-ZENTRUM POTSDAM
DEUTSCHES
GEOFORSCHUNGSZENTRUM

I. Bergmann–Wolf, E. Forootan,
V. Klemann, J. Kusche, H. Dobslaw

Updating ESA's Earth System Model for Gravity Mission Simulation Studies

3. A Realistically Perturbed Non-Tidal Atmosphere and Ocean De-Aliasing Model

Scientific Technical Report STR14/09

www.gfz-potsdam.de

HELMHOLTZ
GEMEINSCHAFT

Recommended citation:

Bergmann-Wolf, I., Forootan, E., Klemann, V., Kusche, J., Dobslaw, H. (2015),
Updating ESA's Earth System Model for Gravity Mission Simulation Studies: 3. A Realistically Perturbed Non-Tidal Atmosphere and Ocean De-Aliasing Model. *Scientific Technical Report 14/09, GFZ German Research Centre for Geosciences*.
DOI: http://doi.org/10.2312/GFZ.b103-14091.

Imprint

Helmholtz Centre Potsdam
GFZ German Research Centre for Geosciences

Telegrafenberg
D-14473 Potsdam

Published in Potsdam, Germany
March 2015

ISSN 2190-7110

DOI: 10.2312/GFZ.b103-14091
URN: urn:nbn:de:kobv:b103-14091

This work is published in the GFZ series
Scientific Technical Report (STR)
and electronically available at GFZ website
www.gfz-potsdam.de

ESA Contract No. 4000109421

Updating ESA's Earth System Model for Gravity Mission Simulation Studies

3. A Realistically Perturbed Non-Tidal Atmosphere and Ocean De-Aliasing Model

Doc. No.: ESAESM_ND3_i2r0
Issue: 2
Revision: 0
Date: March 23, 2015
Authors: I. Bergmann-Wolf, E. Forootan, V. Klemann, J. Kusche, H. Dobslaw
ESA TO: R. Haagmans (ESTEC)

GFZ Potsdam, Department Geodesy and Remote Sensing

ESA Study Contract Report

ESA Contract No	Subject		Contractor
4000109421	Updating ESA's Earth System Model for Gravity Mission Simulation Studies		GFZ German Research Centre for Geosciences
ESA CR No	**STAR CODE**	**No. of Volumes:** 3 **This is Volume No.** 3	**Contractors Reference**

Abstract

The ability of any satellite gravity mission concept to monitor mass transport processes in the Earth system is typically tested well ahead of its implementation by means of various simulation studies. Those studies often extend from the simulation of realistic orbits and instrumental data all the way down to the retrieval of global gravity field solution time-series. Basic requirement for all these simulations are realistic representations of the spatio-temporal mass variability in the different sub-systems of the Earth as a source model for orbit computations.

For such simulations, a suitable source model is required to represent (i) high-frequency (i.e., sub-daily to weekly) mass variability in the atmosphere and oceans, in order to realistically include the effects of temporal aliasing due to non-tidal high-frequency mass variability into the retrieved gravity fields. In parallel, (ii) low-frequency (i.e., monthly to interannual) variability needs to be modelled with realistic amplitudes, particularly at small spatial scales, in order to assess to what extent a new mission concept might provide further insight into physical processes currently not observable.

The new source model documented here attempts to fulfil both requirements: Based on ECMWF's recent atmospheric reanalysis ERA-Interim and corresponding simulations from numerical models of the other Earth system components, it offers spherical harmonic coefficients of the time-variable global gravity field due to mass variability in atmosphere, oceans, the terrestrial hydrosphere including the ice-sheets and glaciers, as well as the solid Earth. Simulated features range from sub-daily to multiyear periods with a spatial resolution of spherical harmonics degree and order 180 over a period of 12 years. In addition to the source model, a de-aliasing model for atmospheric and oceanic high-frequency variability with augmented systematic and random noise is required for a realistic simulation of the gravity field retrieval process, whose necessary error characteristics are discussed.

The documentation is organized as follows: The characteristics of the updated ESM along with some basic validation are presented in Volume 1 of this report (Dobslaw *et al.*, 2014). A detailed comparison to the original ESA ESM (Gruber *et al.*, 2011) is provided in Volume 2 (Bergmann-Wolf *et al.*, 2014), while Volume 3 (Bergmann-Wolf *et al.*, 2015) contains a description of a realistically perturbed de-aliasing model for the high-frequency mass variability in atmosphere and oceans.

The files of the updated ESA Earth System Model for gravity mission simulation studies are accessible at DOI:10.5880/GFZ.1.3.2014.001.

Authors:
I. Bergmann-Wolf, E. Forootan, V. Klemann, J. Kusche, H. Dobslaw

Name of ESA study Manager	ESA Budget Heading
Roger Haagmans Section: Earth Surfaces and Interior Section Division: Mission Science Division Department: Science, Application and Future Technologies	

Scientific Technical Report STR14/09, Deutsches GeoForschungsZentrum GFZ. http://doi.org/10.2312/GFZ.b103-14091

Contents

List of Figures

Chapter 1

Introduction

Current state-of-the-art gravity field retrieval methods applied to GRACE sensor data require a priori background information on high-frequency mass variability in atmosphere and ocean. For GRACE, this knowledge is typically taken from the Atmosphere and Ocean Level-1B De-aliasing Product (AOD1B; Flechtner & Dobslaw, 2013) routinely processed by the GRACE Science Data System. The most recent release 05 of AOD1B is a set of 6-hourly products developed up to spherical harmonic degree and order (d/o) 100, which is based on operational ECMWF analysis atmospheric fields and ocean-bottom pressure as simulated with the numerical ocean model OMCT forced by ECMWF atmospheric data (Dobslaw *et al.*, 2013).

Information currently available from AOD1B is, however, not perfectly correct, even though a substantial increase in accuracy has been realized during the GRACE mission period. Despite of those improvements, de-aliasing errors are still assumed to be one of the major obstacles for reaching the GRACE accuracy baseline (e.g., Zenner *et al.*, 2014). This implies that such errors need to be included at a realistic level also in end-to-end simulation studies for future satellite gravity missions.

Various strategies have been adopted in the past to include errors of the time-variable background models into future mission simulations in a realistic way. Frequently, differences between independent models are assumed to be an acceptable approximation (Wiese *et al.*, 2009, 2012; Loomis *et al.*, 2011). Those differences usually originate from two models only and are not analyzed in great detail. Common model assumptions or a differing treatment of atmospheric tides might therefore lead to overly low or overly high model differences, respectively, with consequences for the conclusions drawn out of the simulations on the relative importance of de-aliasing errors. Alternatively, a fraction of, e.g., 10% of the signal is sometimes assumed as error for the background model (Visser, 2010; Elsaka *et al.*, 2014). While it is reasonable to assume that background model errors are in particular high where strong mass variability is present, this approach does not account for contributions from systematic weaknesses and biases of the chosen atmosphere and ocean mass variability model.

To reduce uncertainties introduced into satellite gravity simulation studies from those widely differing choices for the de-aliasing errors and to provide a common framework for upcoming simulation studies, we are going to re-assess in this report several contributors to the overall background error model budget for non-tidal mass variability in atmosphere and oceans. First, mass variability signals from physical processes that are currently omitted by AOD1B are investigated. Secondly, we quantify pairwise differences of four different ocean and atmosphere models to assess the uncertainties of large-scale non-tidal mass variability at in total five different frequency bands that cover all periods from 6 hours to 30 days. Thirdly, mass variability at small spatial scales typically not treated by global atmospheric and oceanic models is assessed from a high-resolution regional atmo-

spheric model over Europe, whose effects are extrapolated to the globe by means of an empirically derived relation to the roughness of the local topography.

To allow for a straightforward and flexible implementation of the background model errors introduced above, we derive two different sets of spherical harmonic coefficients that are made publicly available at DOI:10.5880/GFZ.1.3.2014.001 together with the source model coefficients of the updated ESA Earth System Model (Dobslaw *et al.*, 2015). 'DEAL' coefficients differ from 'AO' of the source model only by means of the physical processes currently also omitted in AOD1B. 'AOerr' coefficients represent a series of true errors as the sum of both large-scale and small-scale errors with zero mean and stationary variance, that can be added to the 'DEAL' coefficients in order to arrive at a realistically perturbed background model. Both sets of coefficients are given in the same format as the updated ESM and with the same temporal and spatial resolution.

Providing those two separate components of the error model offers flexibility for users: For example, 'DEAL' might be easily replaced by 'AO' of the source model in case that good reasons exist to assume that omitted physical processes will be included in geophysical models available at the anticipated launch date of a future mission. At the same time, 'AOerr' might be re-scaled by an arbitrary constant factor in order to account for anticipated future improvements in the accuracy of those models until launch.

The present report is structured as follows: Dynamical processes in atmosphere and oceans that are currently omitted in AOD1B are discussed in Ch. 2. Large-scale errors based on pairwise model comparisons are evaluated for periods of 10 – 30 days (Ch. 3), 3 – 10 days (Ch. 4), 1 – 3 days (Ch. 5), the S1 atmospheric tide at 24 hours (Ch. 6) and sub-diurnal periods (Ch. 7). Errors at small spatial scales typically not treated by global models are assessed in Ch. 8, before a summary on the error model is presented in the final Ch. 9.

Chapter 2

Error Contributions Due to Missing Physical Processes

2.1 Physical Processes not Represented by GRACE AOD1B

The atmospheric mass variability for the GRACE Atmosphere and Ocean De-Aliasing Product (AOD1B) (Flechtner & Dobslaw, 2013) is derived from operational ECMWF analysis fields with a 6 hourly sampling. Those analyses are based on a state-of-the-art global numerical weather prediction model that includes all dynamical processes relevant for the description of transient weather systems down to spatial scales of several km. Moreover, ECMWF assimilates many types of both satellite and in-situ observations, making the finally provided atmospheric pressure, temperature, and humidity fields highly realistic. Although the presence of errors in ECMWF cannot be excluded, we assert that there are no known missing physical processes in the atmospheric part of AOD1B that would be relevant for the objective of this study.

The ocean part of AOD1B, however, is based on an unconstrained version of the global numerical ocean circulation model OMCT (Thomas *et al.*, 2001). The model is discretized on a regular 1° grid and is therefore limited to the simulation of regional-scale signals only and does not allow to represent meso-scale variability. In addition, eddy variability typically arises from baroclinic instabilities, where the timing and the exact position of the initialization of meso-scale turbulences is not predictable deterministically from the knowledge of atmospheric conditions alone, as it is otherwise possible for wind- and pressure-driven ocean-bottom pressure signals.

Eustatic variations of global mean sea-level are caused by the re-distribution of freshwater between continental and oceanic storages. Although model predictions of eustatic sea-level variability are principally available (Dobslaw & Thomas, 2007), it has been decided to exclude this process from AOD1B by keeping the total ocean mass intentionally constant at every time instance, and we apply this convention also within the de-aliasing model provided for the updated ESM.

2.2 A Time-Series of Unperturbed De-Aliasing Coefficients: DEAL

Based on the arguments presented above, we derive the de-aliasing model for the updated ESM from the OMCT simulations developed up to $\mathrm{d/o} = 180$, where the total ocean mass is kept constant at every time-step by adding or removing a homogeneous layer of mass over all ocean grid points. In contrast to the updated ESM, no replacement of the $\mathrm{d/o} > 60$ with results from the MPIOM STORM experiment (Storch *et al.*, 2012) is made.

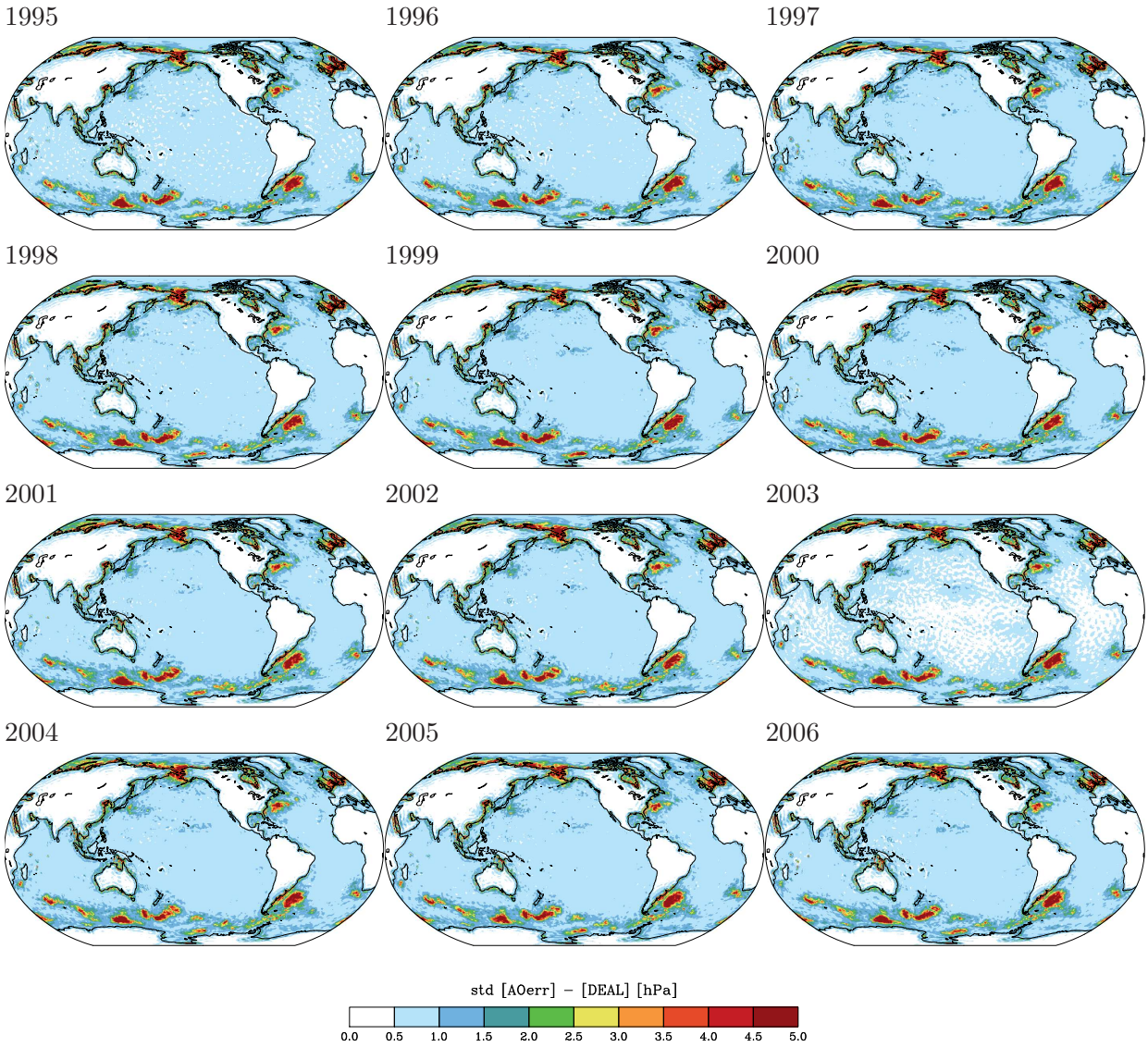

Figure 2.1: Rms of bottom pressure anomalies caused by physical processes that are intentionally omitted in currently available de-aliasing models for individual years 1995 – 2006.

Rms differences between the sum of the A+O components of the updated ESM and the de-aliasing model (Fig. 2.1) indicate the level of variability in atmosphere and ocean that can be predicted from a deterministic model combination for spatial scales of d/o $\geq$ 60 over the oceans under ideal conditions provided that only ocean models that do not assimilate observational data are available. Differences are zero over the continents, and reach up to 10 hPa (corresponding to 10 cm of equivalent water thickness) in coastal regions and over oceanic areas characterized by high eddy kinetic energy. Signals are, however, dominated by rather small spatial scales, suggesting that the contribution of errors due to omitted physical processes to the overall de-aliasing error budget of a satellite gravity mission is not too large.

For completeness we show also global degree variances of differences between the source and the de-aliasing model (Fig. 2.2). As expected, variance substantially increases at d/o = 60, where MPIOM STORM information is introduced into the updated ESM for the first time. The spectral characteristics do not vary too much from year to year, thereby underlining once more the stationarity of the model. Peaks in the spectrum present in every year are in particular related to the coast line distribution, where most of the variability resides.

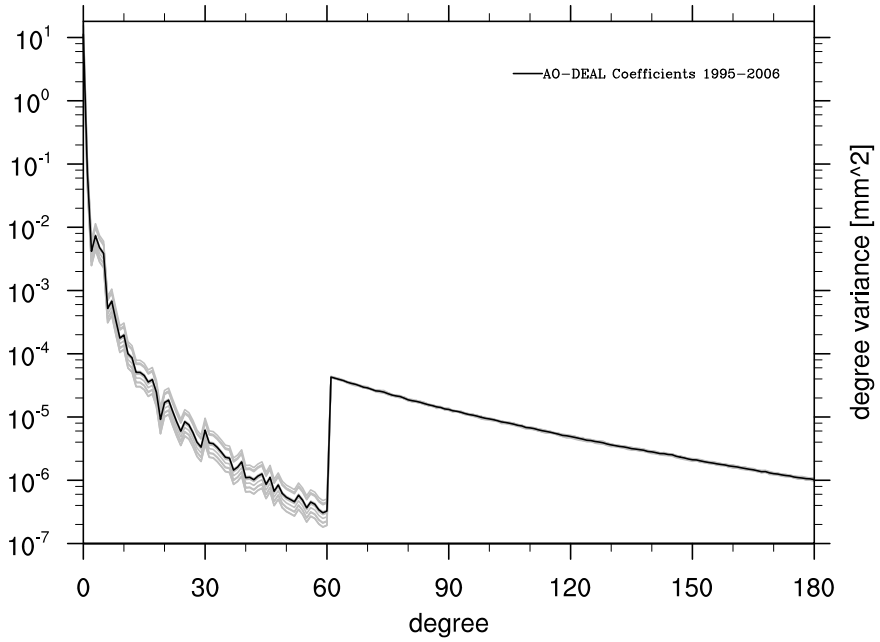

Figure 2.2: Degree variances of physical signals that are intentionally omitted in de-aliasing models: averaged over 12 years (black) and for individual years 1995 – 2006 (grey).

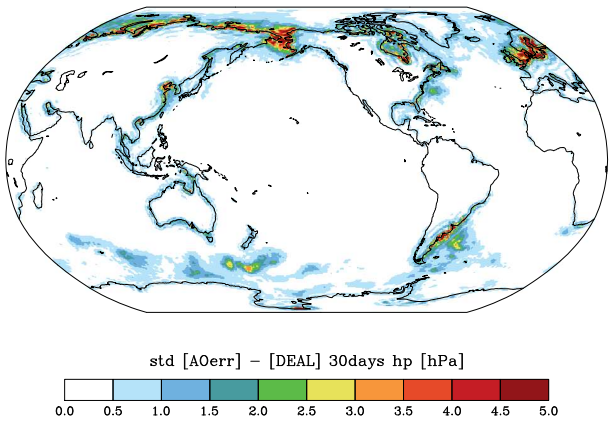

Figure 2.3: Rms of bottom pressure anomalies caused by physical processes that are intentionally omitted in currently available de-aliasing models with periods shorter than 30 days averaged over the years 1995 – 2006.

We argued before that a large fraction of the oceanic signals conventionally omitted in de-aliasing models are dominated by seasonal and even longer periods. To demonstrate this more explicitly, we filter the difference between the source model of the updated ESM and the unperturbed de-aliasing coefficients with a 3rd order Butterworth high-pass filter with a 30 days cutoff period (Fig. 2.3). Variations in total ocean mass leading to changes in eustatic sea-level are found to be vanished. Signals from meso-scale ocean dynamics are still present but are largely reduced, justifying the omission of those processes from present-day de-aliasing models. Coastal processes are, however, still large and potentially contribute to some extent to the aliasing errors in the final monthly-mean gravity field solutions. Since de-aliasing model presently available do not provide very high-resolution, such coastal processes are only poorly represented and errors along the coasts are consequently expected to be higher than in the open ocean. We therefore conclude that increased error levels along the coasts are a reasonable feature of the unperturbed de-aliasing coefficients.

Chapter 3

Errors with Large Spatial Scales at Periods of 10 – 30 days

3.1 Strategy for the Error Approximation from Re-scaled Model Differences

De-aliasing errors at large spatial scales are characterized by strong spatial and temporal correlations that differ substantially with geographic position. Such features are difficult to model as a stochastic process in the absence of independent information on, e.g., correlation lengths, and we therefore approximate them from differences between two model realizations of atmospheric and oceanic mass variations that are properly scaled to compensate for biases common to both models.

We have two series of atmospheric and oceanic mass variability at hand that cover the full 12 year period, namely the original ESA Earth System Model (Gruber *et al.*, 2011), and the updated ESM (Dobslaw *et al.*, 2015). To distinguish between different frequency bands, we apply bandpass filtering with 3rd order Butterworth filters with different cut-off periods to the gridded model differences. Filtered model differences are subsequently scaled with constant factors for continental and oceanic grid points, respectively, as distinguished by the AOD1B land-ocean mask.

To quantify the scaling coefficients, we rely on a pairwise model comparison of mass variability in atmosphere and ocean from four different global atmosphere and ocean models over the year 2006. ERA-Interim (Dee *et al.*, 2011) is the most recent global atmospheric re-analysis of the European Centre for Medium-Range Weather Forecasts (ECMWF) that is also used for the updated ESM. The Climate Forecast System Reanalysis (CFSR; Saha *et al.*, 2010) has been prepared by the National Center for Environmental Prediction in the U.S., and we are also using NASA's Modern Era Retrospective Analysis for Research and Applications (MERRA; Rienecker *et al.*, 2011). The fourth atmospheric dataset we have at hand are the operational ECMWF analyses that are also included in AOD1B.

For the oceans, we assess the most recent simulation from OMCT (Dobslaw *et al.*, 2013) forced with ERA-Interim atmospheric data, the MPIOM STORM experiment with NCEP2 forcing (Storch *et al.*, 2012), and a version of the French TUGO model (Carrère & Lyard, 2003; Le Bars *et al.*, 2010) forced with ERA-Interim as it is contained in the alternative GRACE de-aliasing model provided by GRGS. Finally, we utilize a recent experiment from the ECCO2 ocean synthesis produced at JPL (cube92; Menemenlis & Campin, 2008) that assimilates a vast range of different oceanographic observations. While deriving scaling coefficients from these pairwise comparisons, we implicitly assume that all model fields available represent erroneous realizations of a single mean truth, and all have approximately similar error levels. The selection of those coefficients

is always based on a comparison of the ensemble of pairwise model differences from 2006 with the rms differences between the original and the updated ESM over all 12 years available. By this, we make sure that the error series provided reflects on average over the 12 years of the updated ESA ESM the spread among four present-day models.

Errors at periods of 30 days and longer will not contribute to the actual de-aliasing errors. Instead, they will directly enter into the estimated monthly mean gravity field, which is the 'GSM' field in the terminology of the GRACE Science Data System. To assess bottom pressure variability from GRACE, it is required to restore the monthly mean of the applied de-aliasing model that is provided along with 'GSM' as the so-called 'GAC' field. Thus, errors of periods of 30 days or longer are perfectly compensated by re-adding 'GAC', and therefore do not need to be included into the error model for the de-aliasing. For the atmosphere, such errors would principally enter additively to 'GSM' without, however, causing artifacts, i.e., meridional stripes. We therefore conclude that it is acceptable to ignore errors of periods longer than 30 days in the high-frequency de-aliasing products also over the continents.

We note, however, that errors occurring at periods longer than 30 days will inevitably be interpreted as continental water mass anomaly in the monthly mean observation results inferred from sensor data of a GRACE-type satellite gravity mission. In Forootan *et al.* (2014) for instance, an improved set of 6-hourly atmospheric de-aliasing products was used to assess the computations of linear trends as well as the amplitude of annual and semi-annual mass changes from GRACE-derived mass estimations. Further experiments with this improved de-aliasing product in contrast to the standard AOD1B might be used to demonstrate that errors at periods larger than 30 days indeed do not contribute to stripes in a particular gravity field estimation strategy intended to be used for a simulation study.

3.2 Multi-Model Comparison for 2006

In order to assess the current level of uncertainties in global models of atmospheric mass variability, we calculate pairwise rms atmospheric model differences that are bandpass filtered to contain only variability with periods of 10 – 30 days over the year 2006 (Fig. 3.1). For closely related model pairs, as for example operational and re-analysis data from ECMWF, we note globally fairly homogeneous residuals of about 0.2 hPa only. The spread is substantially larger when European models are compared with American realizations, culminating in rms differences of up to 0.7 hPa in Antarctica. Based on the pairwise model comparison, we conclude that differences between the original and the updated ESM underestimate the uncertainty. We therefore up-scale the atmospheric component by 150% for the period band of 10 – 30 days (Fig. 3.2).

For the ocean component, we note rather small differences between STORM and ECCO2 that both lack forcing from atmospheric pressure variability and thus miss a small but non-negligible part of the energy input from the atmosphere into the oceans (Fig. 3.3). This is in particular relevant for the Arctic Ocean, where the inverse barometric adjustment to atmospheric pressure changes is hampered by the narrow straits connecting the basin to the Pacific and the North Atlantic. Residuals for all model differences show a clear zonal structure, where larger errors are found in regions with larger signal variability. Based on these comparisons, we conclude that the uncertainty associated with ocean bottom pressure variability for the period band of 10 – 30 days is well represented by the un-scaled ESM model difference (Fig. 3.4).

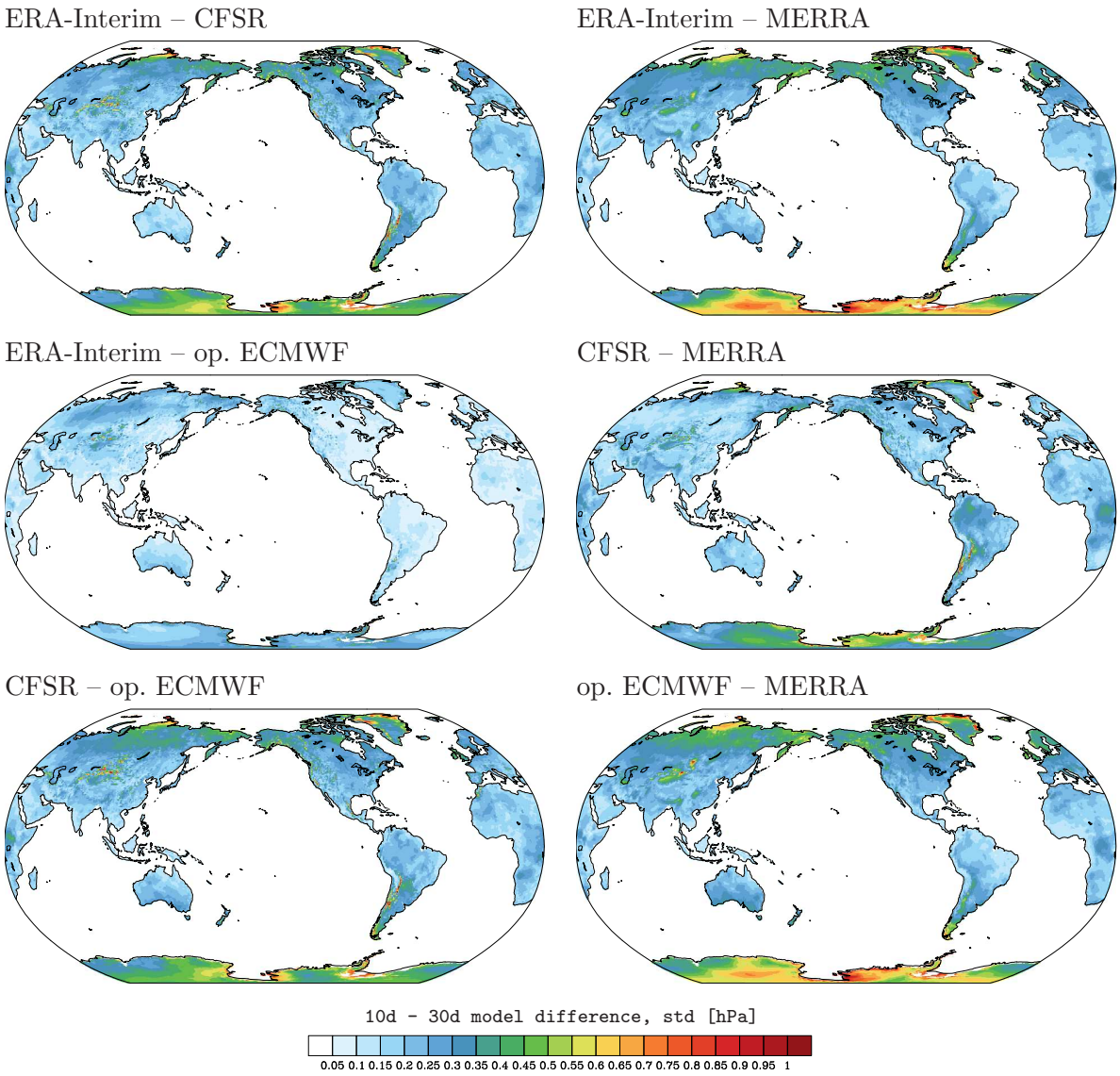

Figure 3.1: Rms differences of band-pass filtered atmospheric mass variability from four different global atmospheric surface pressure data-sets at periods of 10 – 30 days: ERA-Interim re-analysis, MERRA re-analysis, CFSR re-analysis, and ECMWF operational analyses.

3.3 Re-scaled Error Estimates for 1995 – 2006

Model differences that are bandpass filtered for periods of 10 – 30 days with a 3rd order Butterworth filter and re-scaled individually for atmosphere and oceans are analyzed up to d/o = 180 for all 12 years. Subsequently, coefficients are re-synthesized onto the original 0.5° grid and rms errors for all individual years are calculated. For the atmosphere (Fig. 3.5), we note weak non-stationarity in particular in Antarctica between the first and the second half of the series that is related to the transition from ERA-40 to operational ECMWF in Jan 2001 in the original ESM (Fig. 3.5). For the oceans, we note stronger year-to-year variability with some exceptional features in the southern Pacific around Bellingshausen Basin in 2005 (Fig. 3.6). Degree variances of the combined atmosphere and ocean variability, however, do not reveal substantial differences among the individual years (Fig. 3.7).

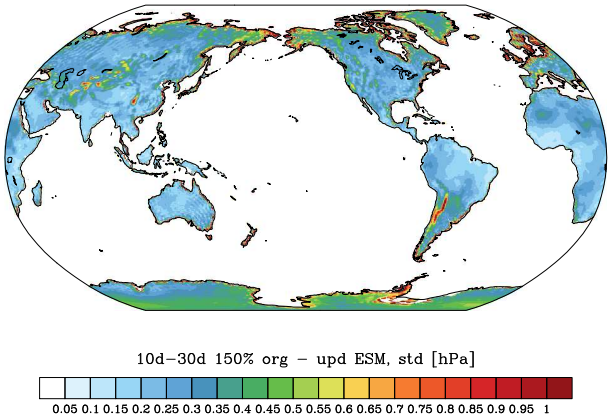

Figure 3.2: Rms differences of re-scaled atmospheric errors over the continents with large spatial scales at periods of 10 – 30 days as averaged over the period 1995 – 2006.

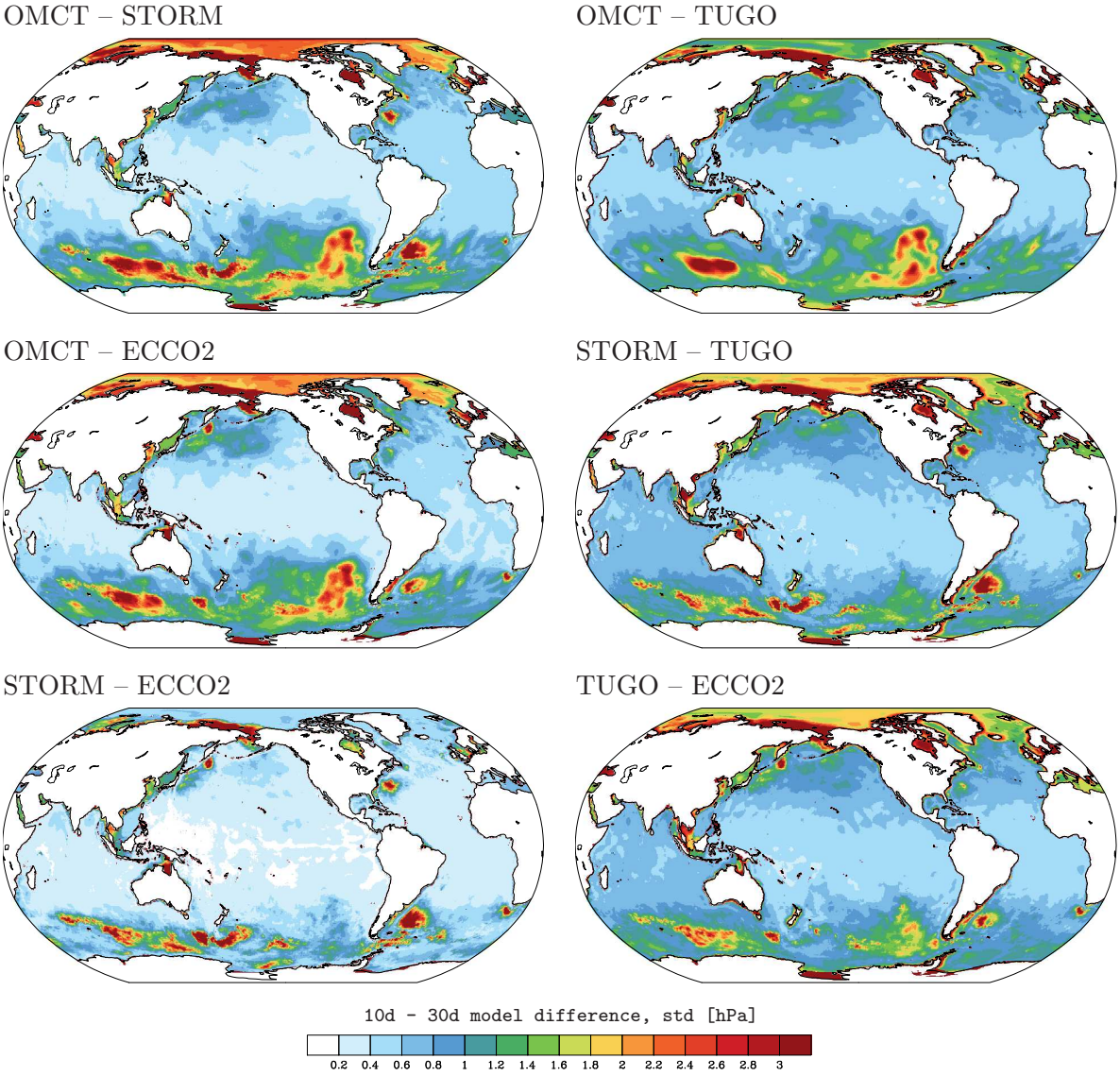

Figure 3.3: Rms differences of band-pass filtered ocean bottom pressure variability from four different global ocean bottom pressure data-sets at periods of 10 – 30 days: OMCT as used for AOD1B RL05, TUGO, ECCO2, and the MPIOM STORM experiment.

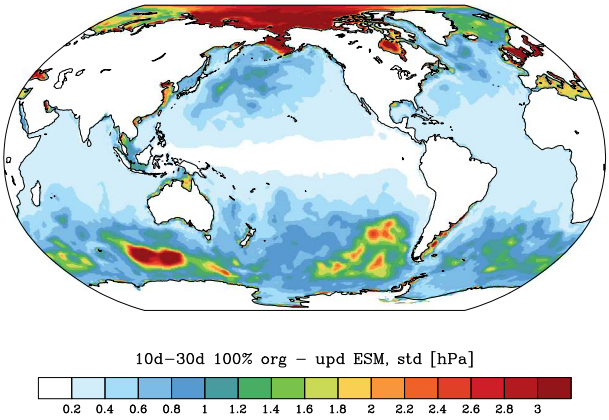

Figure 3.4: Rms differences of re-scaled ocean bottom pressure errors with large spatial scales at periods of 10 – 30 days as averaged over the period 1995 – 2006.

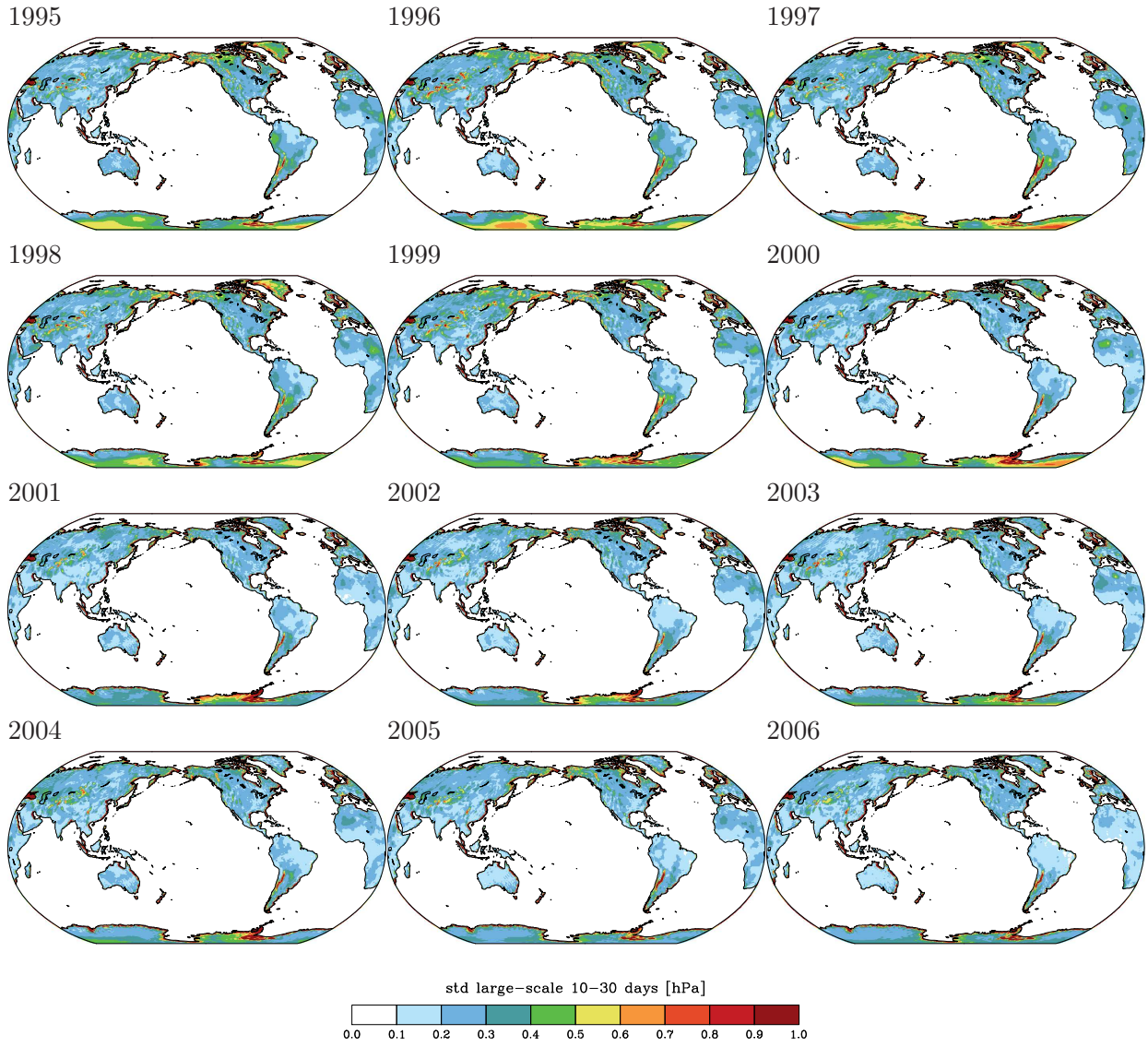

Figure 3.5: Rms of atmospheric errors with large spatial scales over the continents at periods of 10 – 30 days for individual years 1995 – 2006.

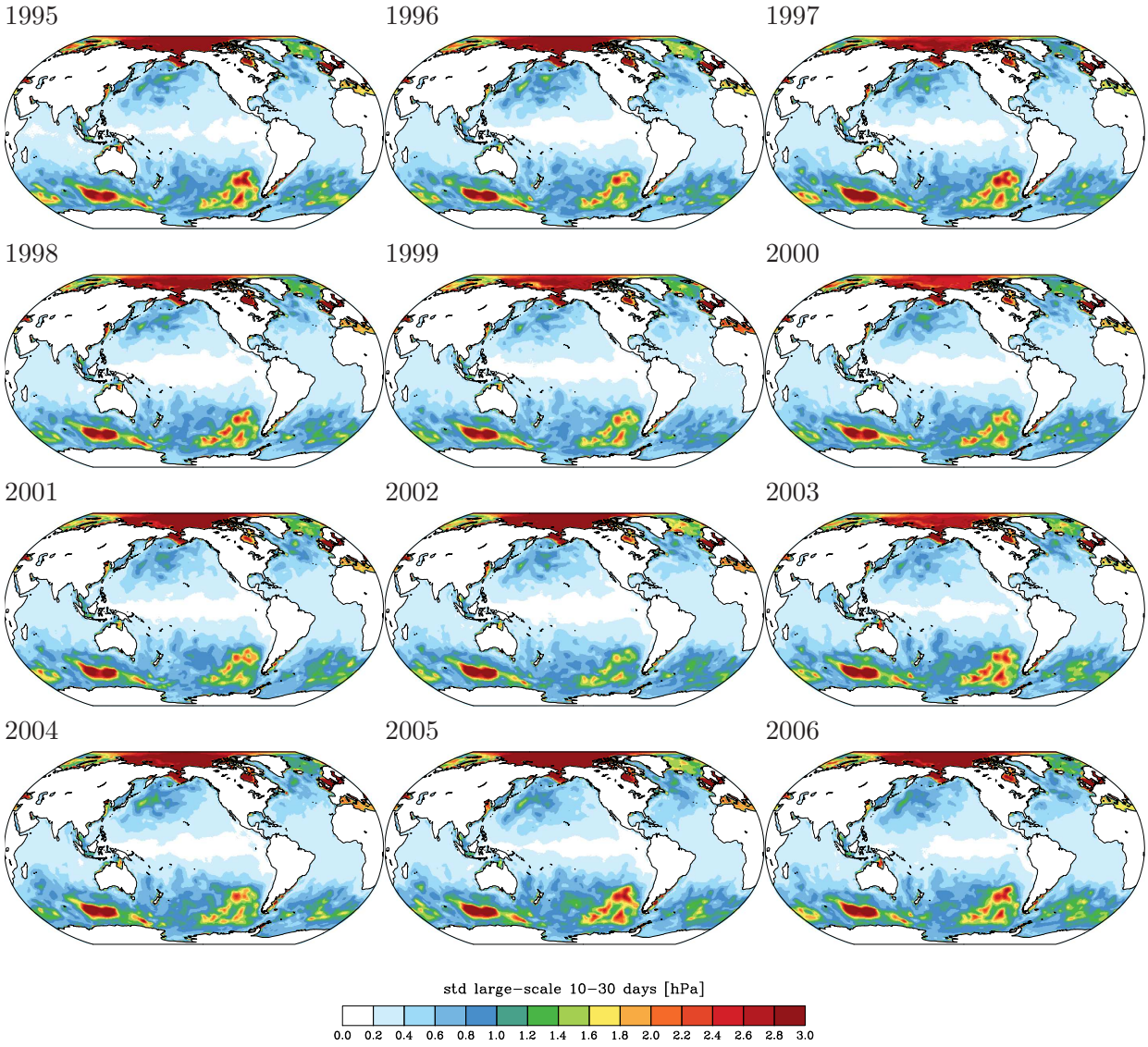

Figure 3.6: Rms of ocean bottom pressure errors with large spatial scales at periods of 10 – 30 days for individual years 1995 – 2006.

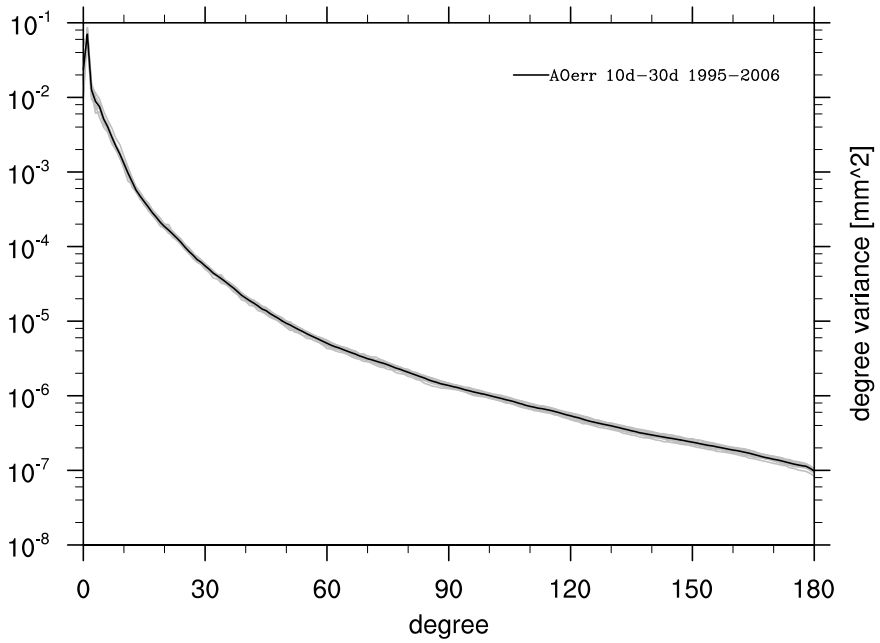

Figure 3.7: Degree variances for re-scaled large-scale true errors of atmosphere and ocean at periods of 10 – 30 days: averaged over 12 years (black) and for individual years 1995 – 2006 (grey).

Chapter 4

Errors with Large Spatial Scales at Periods of 3 – 10 days

4.1 Multi-Model Comparison for 2006

Pairwise multi-model comparisons are further performed for the bandpass filtered signals at periods of 3 – 10 days. For the atmospheric surface pressure variability over the continents (Fig. 4.1), we note rather large differences between the European models on the one hand side, and the U.S. re-analyses on the other. ERA Interim and the operational ECMWF correspond to each other rather well, with rms differences hardly exceeding 0.3 hPa. Slightly worse correspondence is seen for CFSR and MERRA, that deviate from each other by more than 0.5 hPa only in remote areas as the Himalaya or the Antarctic interior. All other pairs, however, reveal substantially larger discrepancies reaching up to 1 hPa in almost all extra-tropical regions. This is quite plausible since the variability of atmospheric surface pressure in the tropics is much smaller than at higher latitudes in particular at the frequencies considered here. Numerical models tend to diverge more from each other in regions where the signal variability is stronger, and we therefore see a larger spread outside the tropics. Based on those comparisons, we conclude that model differences between the original and the updated ESM need to be scaled over the continents by 250% in order to realistically represent the uncertainties in atmospheric surface pressure variability for periods of 3 – 10 days (Fig. 4.2).

For the ocean bottom pressure variability at periods of 3 – 10 days (Fig. 4.3), we note the best agreement between STORM and ECCO2. This good correspondence is, however, related to missing atmospheric surface pressure forcing in both models. Differences between all other model pairs are substantially larger and have fairly similar regional characteristics. Those include almost no residual signals at tropical latitudes, and very high differences in resonant sub-surface basins in the Southern Ocean and the Arctic. Based on those comparisons, we conclude that the un-scaled ocean bottom pressure differences between the original and the updated ESM represent the uncertainties for periods of 3 – 10 days quite well (Fig. 4.4).

4.2 Re-scaled Error Estimates for 1995 – 2006

Model differences that are bandpass filtered for periods of 3 – 10 days with a 3rd order Butterworth filter and re-scaled with individual constants for atmosphere and oceans are analyzed up to d/o = 180 for all 12 years. Subsequently, coefficients are re-synthesized onto the original 0.5° grid and rms errors for all individual years are calculated. For the atmosphere, we note weak non-stationarity

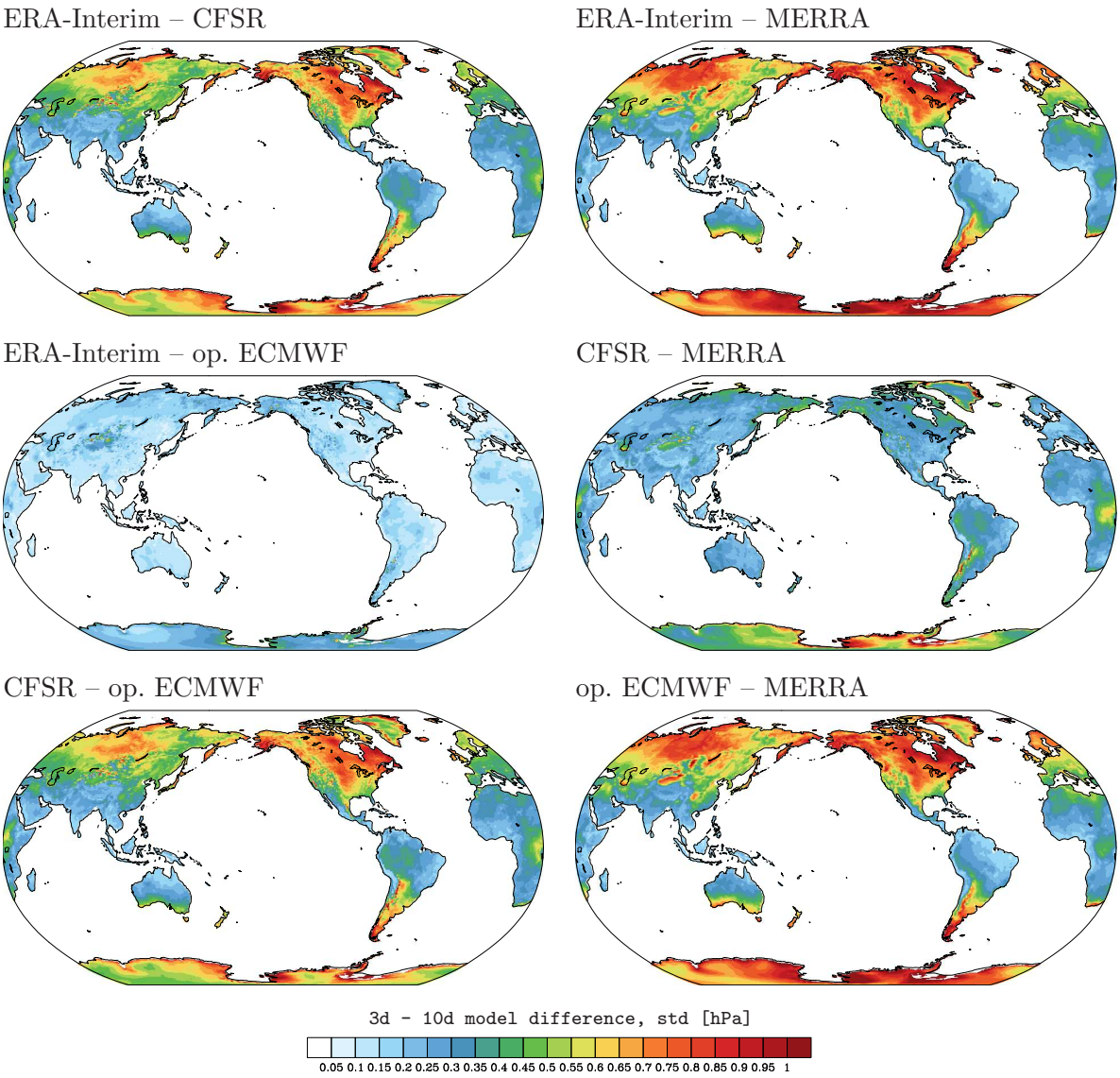

Figure 4.1: Rms differences of band-pass filtered atmospheric mass variability from four different global atmospheric surface pressure data-sets at periods of 3 – 10 days: ERA-Interim re-analysis, MERRA re-analysis, CFSR re-analysis, and ECMWF operational analyses.

between the first and the second half of the series in particular over Greenland, which is related to the transition from ERA-40 to operational ECMWF in Jan 2001 in the original ESM (Fig. 4.5). For the oceans, we note stronger year-to-year variability with some exceptional features in the Arctic Ocean in 2003 (Fig. 4.6). Degree variances of the combined atmosphere and ocean variability, however, do not reveal substantial differences among the individual years (Fig. 4.7).

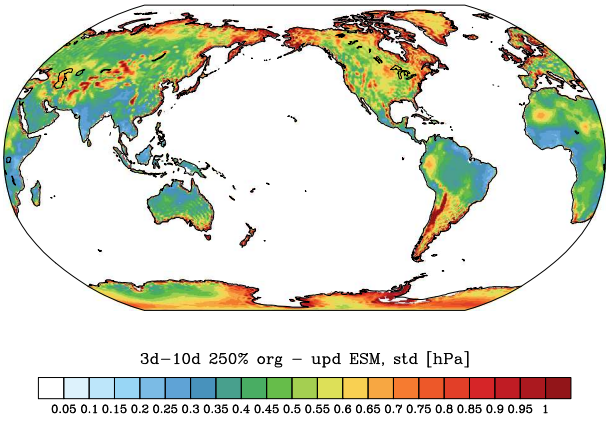

Figure 4.2: Rms differences of re-scaled atmospheric errors over the continents with large spatial scales at periods of 3 – 10 days as averaged over the period 1995 – 2006.

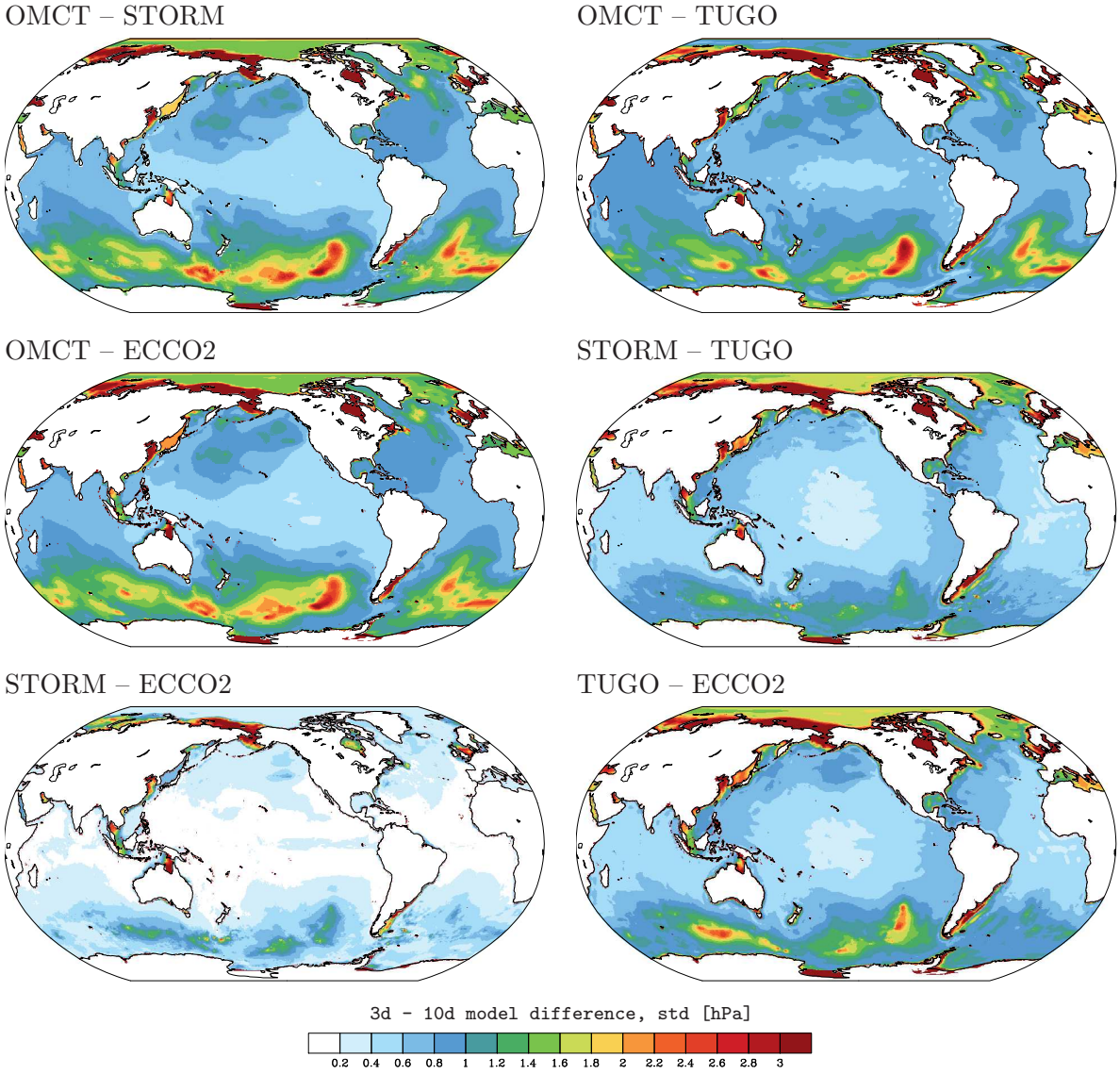

Figure 4.3: Rms differences of band-pass filtered ocean bottom pressure variability from four different global ocean bottom pressure data-sets at periods of 3 – 10 days: OMCT as used for AOD1B RL05, TUGO, ECCO2, and the MPIOM STORM experiment.

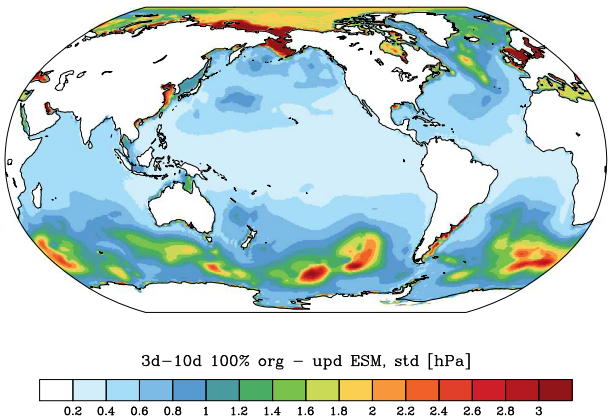

Figure 4.4: Rms differences of re-scaled ocean bottom pressure errors with large spatial scales at periods of 3 – 10 days as averaged over the period 1995 – 2006.

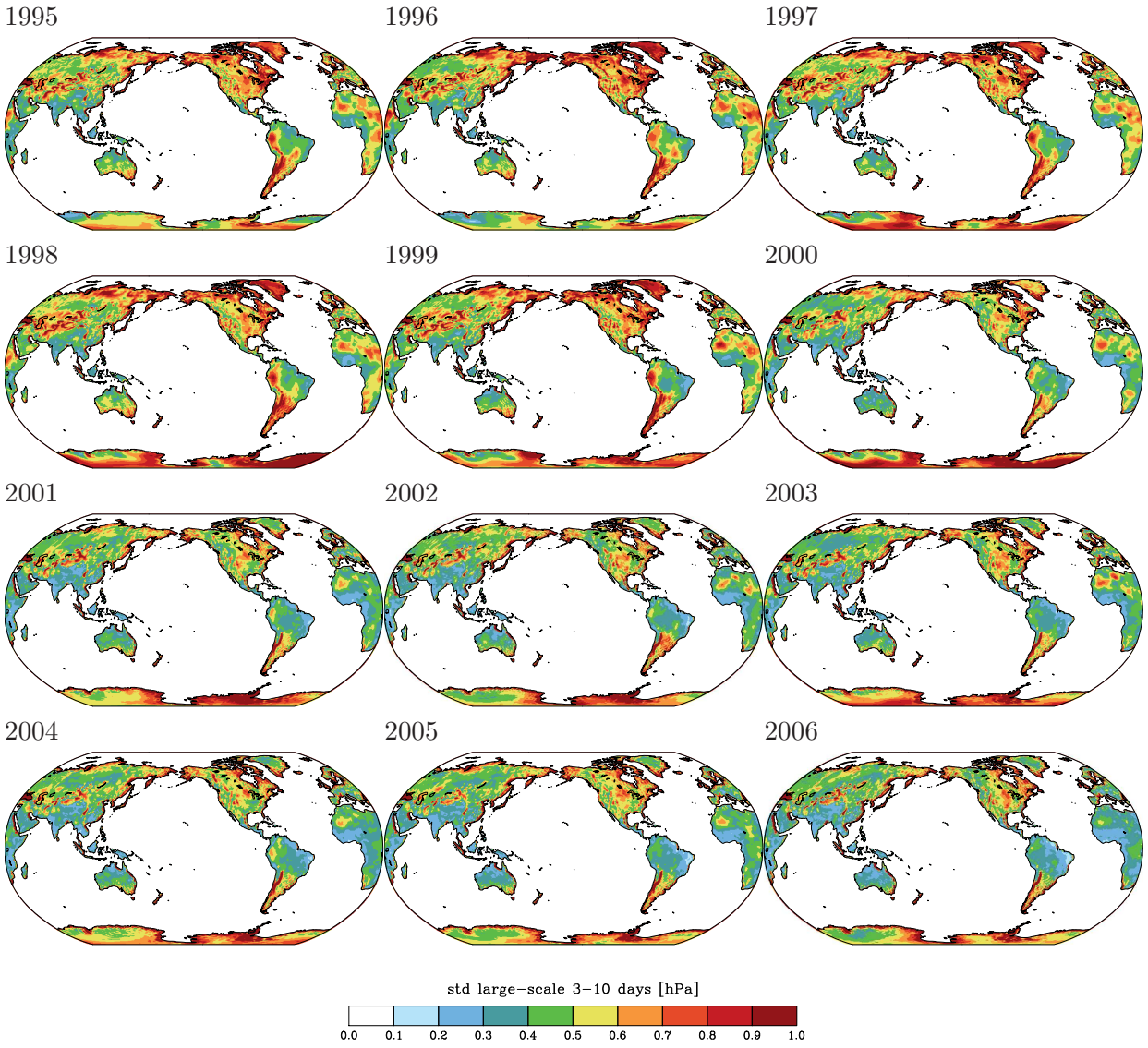

Figure 4.5: Rms of atmospheric errors with large spatial scales over the continents at periods of 3 – 10 days for individual years 1995 – 2006.

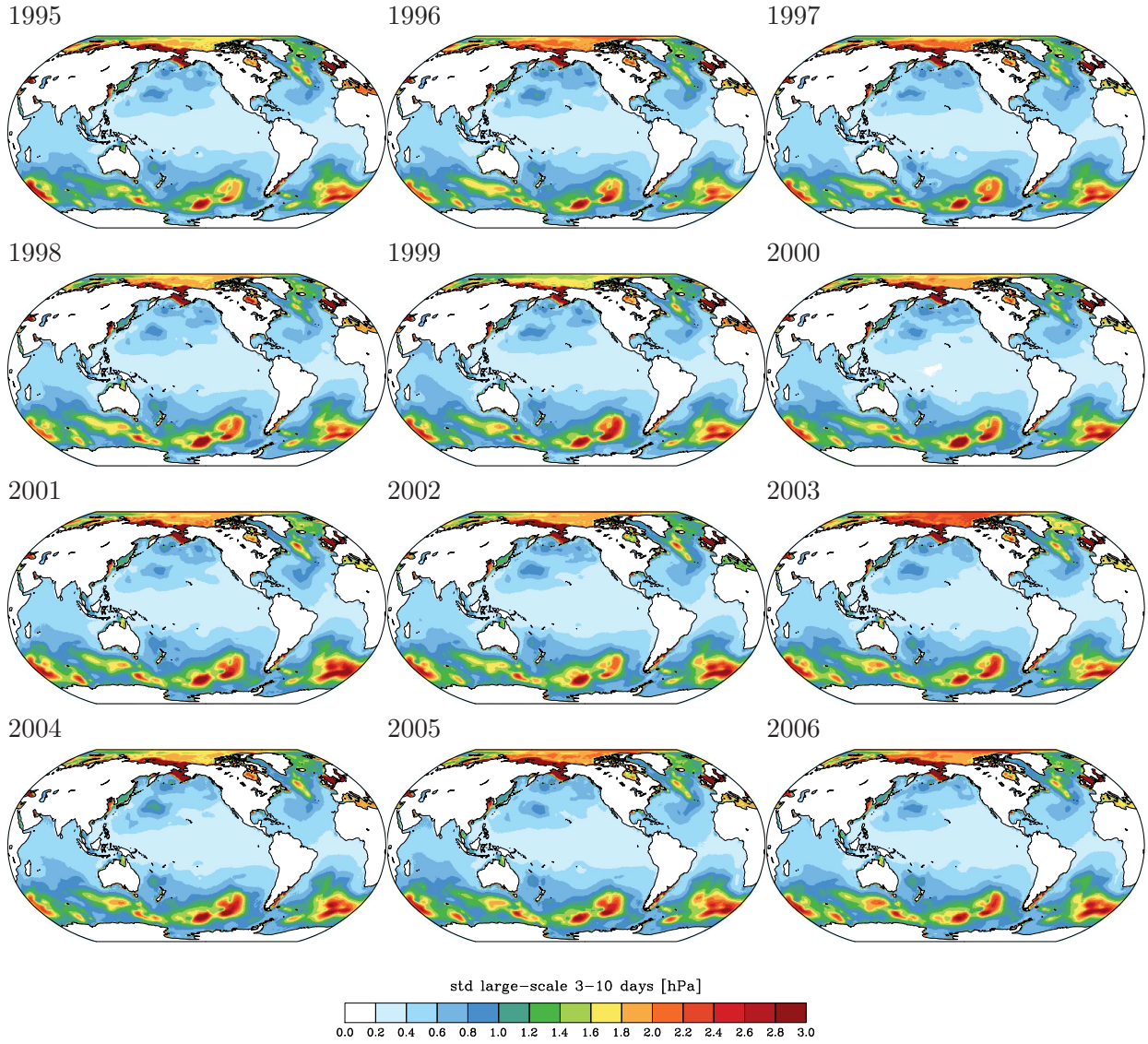

Figure 4.6: Rms of ocean bottom pressure errors with large spatial scales at periods of 3 – 10 days for individual years 1995 – 2006.

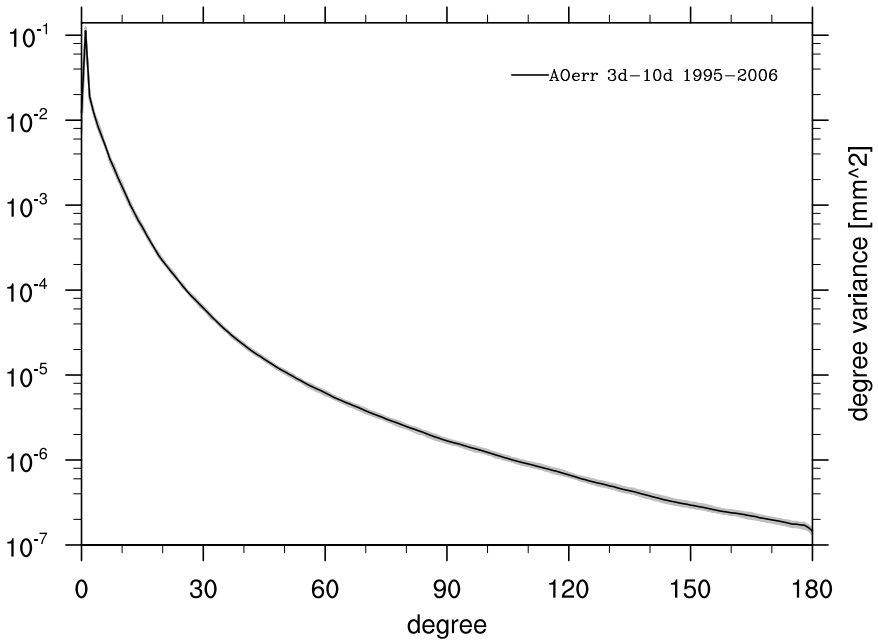

Figure 4.7: Degree variances for re-scaled large-scale true errors of atmosphere and ocean at periods of 3 – 10 days: averaged over 12 years (black) and for individual years 1995 – 2006 (grey).

Chapter 5

Errors with Large Spatial Scales at Periods of 1 – 3 days

5.1 Multi-Model Comparison for 2006

Pairwise multi-model comparisons are performed now for the bandpass filtered signals at periods of 1 – 3 days. For the atmospheric surface pressure variability over the continents (Fig. 5.1), we find again large differences between the U.S. and European models. ERA Interim and the operational ECMWF dataset correspond to each other rather well with rms differences hardly exceeding 0.2 hPa. Slightly worse correspondence is seen for CFSR and MERRA, that deviate from each other by more than 0.4 hPa only in remote areas as the Himalaya or the Antarctic interior. All other model pairs, however, reveal substantially larger discrepancies reaching up to 0.6 hPa in almost all extra-tropical regions.

The spatial pattern of the differences between the original and the updated ESMclearly reflects the difference between ERA-Interim and the operational ECMWF analyses by showing a rather homogeneous level of disagreement over all latitudes. All other model pairs, however, show larger deviations in the extra-tropics, which in principle requires the introduction of latitude-dependent scaling factors. As a compromise, we decided to scale the model differences between the original and the updated ESM over the continents by 350% as a representation of the uncertainties in atmospheric surface pressure variability for periods of 1 – 3 days (Fig. 5.2). By doing so, the errors estimates in the tropics are quite conservative, whereas errors above North America and Central Russia are rather optimistic.

For the ocean bottom pressure variability at periods of 1 – 3 days (Fig. 5.3), we note the best agreement between STORM and ECCO2, which is related again to missing atmospheric surface pressure forcing in both models. Differences between all other model pairs are substantially larger and have fairly similar regional characteristics. Those include almost no residual signals at tropical latitudes, and very high differences in resonant sub-surface basins in the Southern Ocean and in the Arctic. Based on those comparisons, we conclude that the ocean bottom pressure differences between the original and the updated ESM scaled at 150 % represent the uncertainties for periods of 1 – 3 days sufficiently well (Fig. 5.4).

5.2 Re-scaled Error Estimates for 1995 – 2006

Model differences that are bandpass filtered for periods of 1 – 3 days with a 3rd order Butterworth filter and re-scaled with individual constants for atmosphere and oceans are analyzed up to d/o =

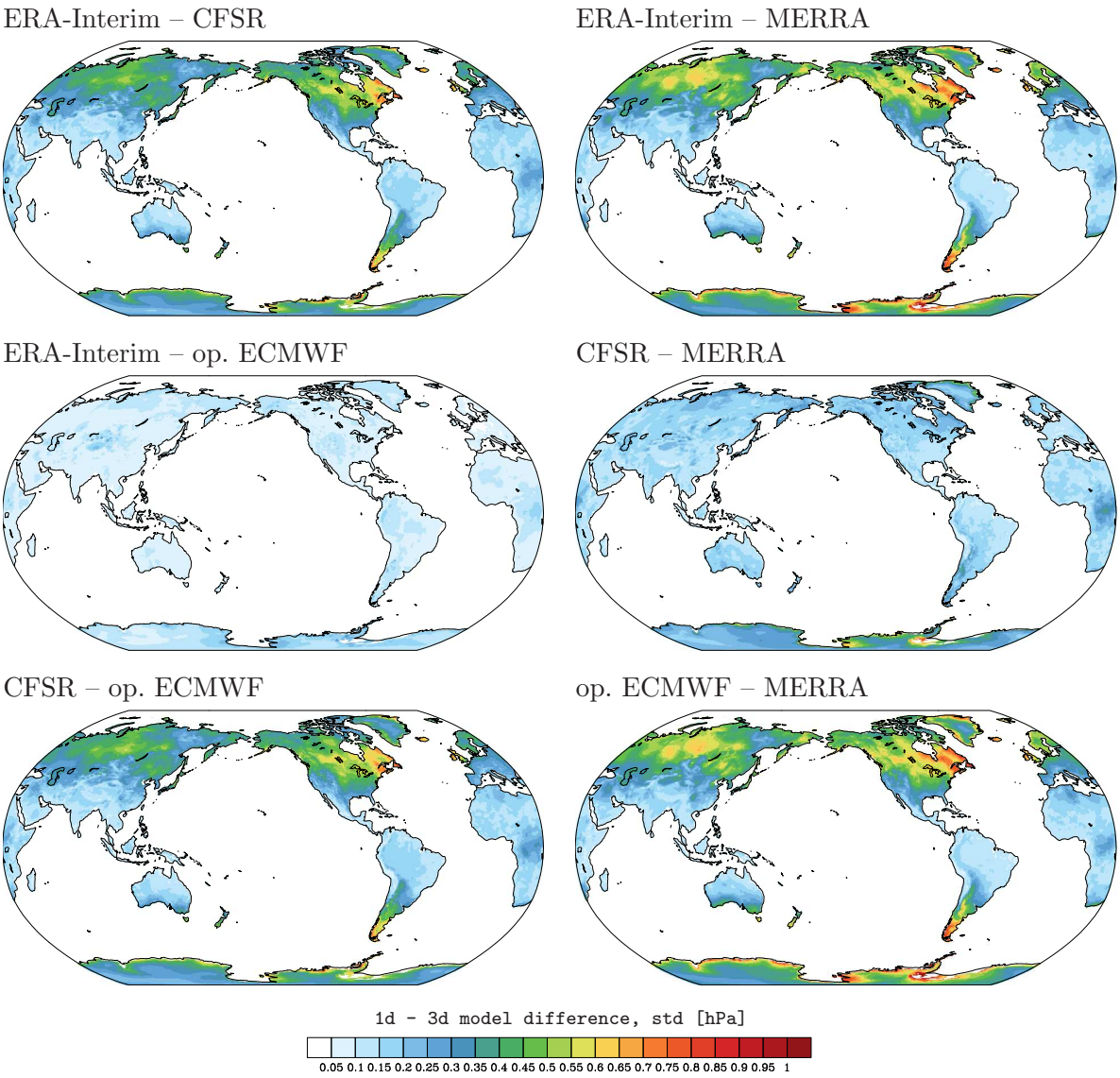

Figure 5.1: Rms differences of band-pass filtered atmospheric mass variability from four different global atmospheric surface pressure data-sets at periods of 1 – 3 days: ERA-Interim re-analysis, MERRA re-analysis, CFSR re-analysis, and ECMWF operational analyses.

180 for all 12 years. Subsequently, coefficients are re-synthesized onto the original 0.5° grid and rms errors for all individual years are calculated. For the atmosphere, we note weak non-stationarity between the first and the second half of the series that are in particular visible in high latitudes of the northern hemisphere (Fig. 5.5). For the oceans, we note stronger year-to-year variability in the Arctic Ocean in the year 1995 (Fig. 5.6). Degree variances of the combined atmosphere and ocean variability, however, do not reveal substantial differences among the individual years (Fig. 5.7).

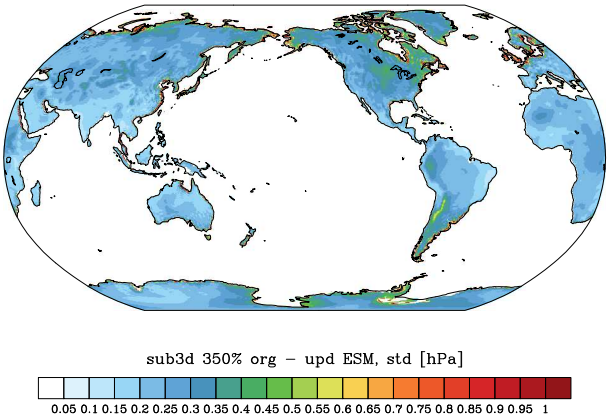

Figure 5.2: Rms differences of re-scaled atmospheric errors over the continents with large spatial scales at periods of 1 – 3 days as averaged over the period 1995 – 2006.

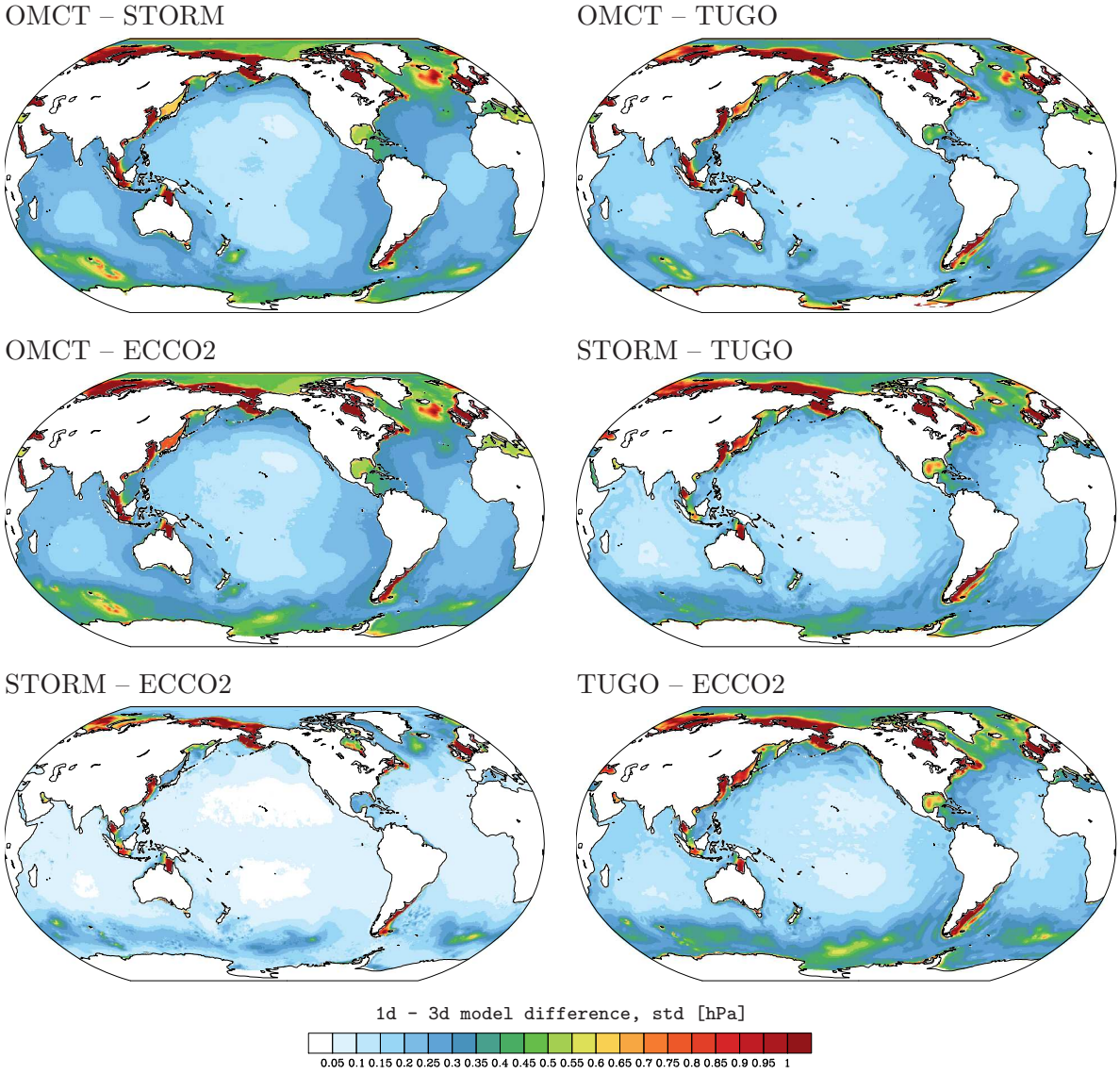

Figure 5.3: Rms differences of band-pass filtered ocean bottom pressure variability from four different global ocean bottom pressure data-sets at periods of 1 – 3 days: OMCT as used for AOD1B RL05, TUGO, ECCO2, and the MPIOM STORM experiment.

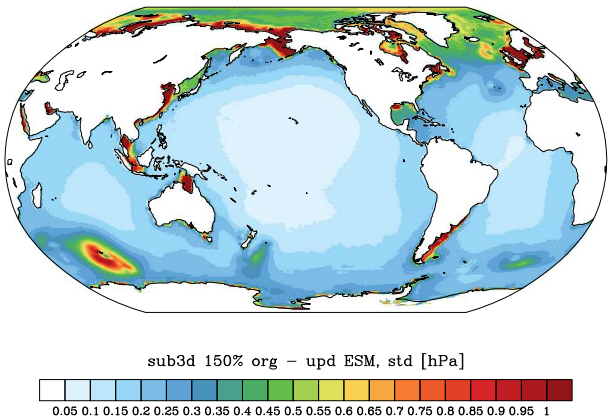

Figure 5.4: Rms differences of re-scaled ocean bottom pressure errors with large spatial scales at periods of 1 – 3 days as averaged over the period 1995 – 2006.

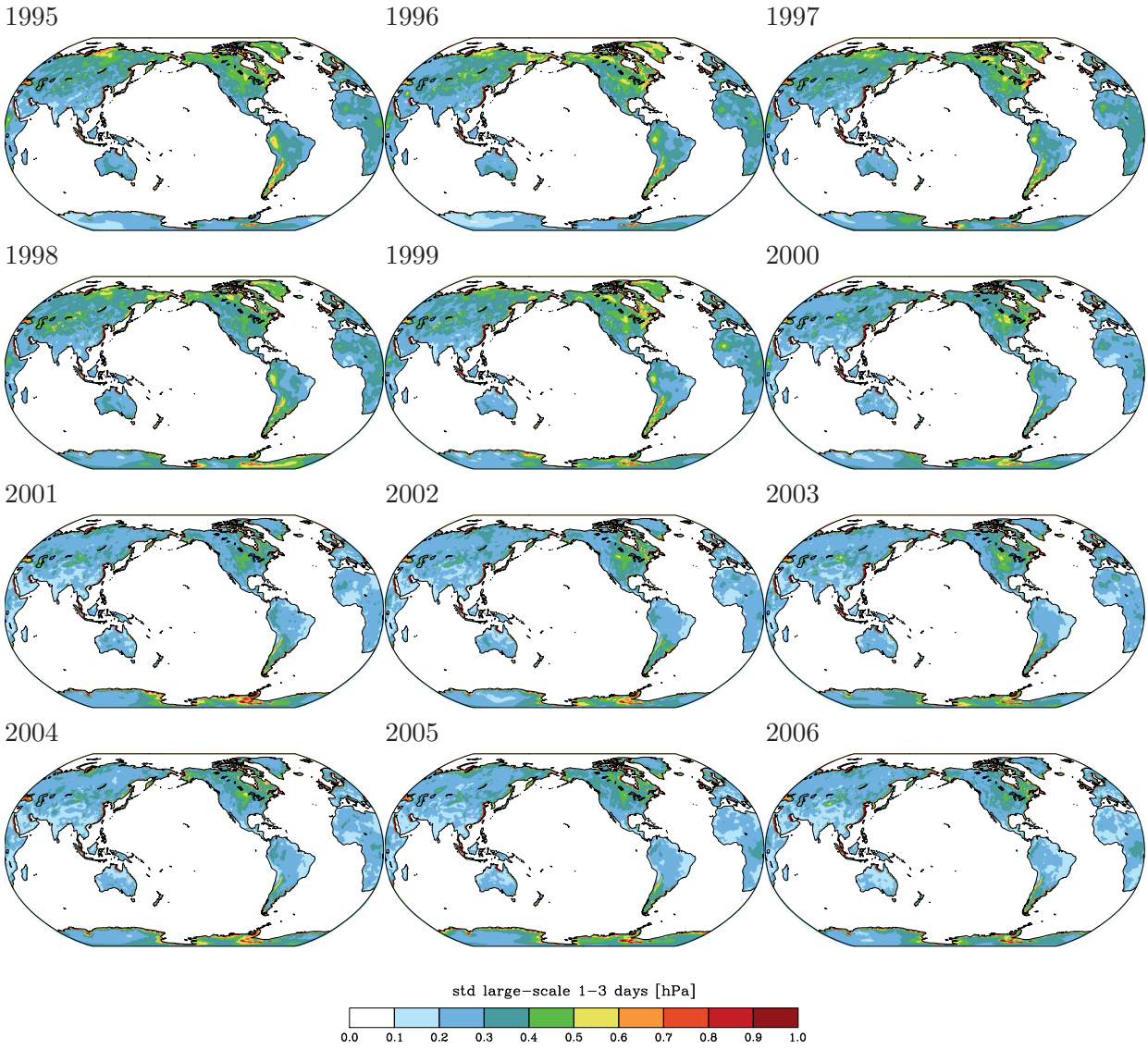

Figure 5.5: Rms of atmospheric errors with large spatial scales over the continents at periods of 1 – 3 days for individual years 1995 – 2006.

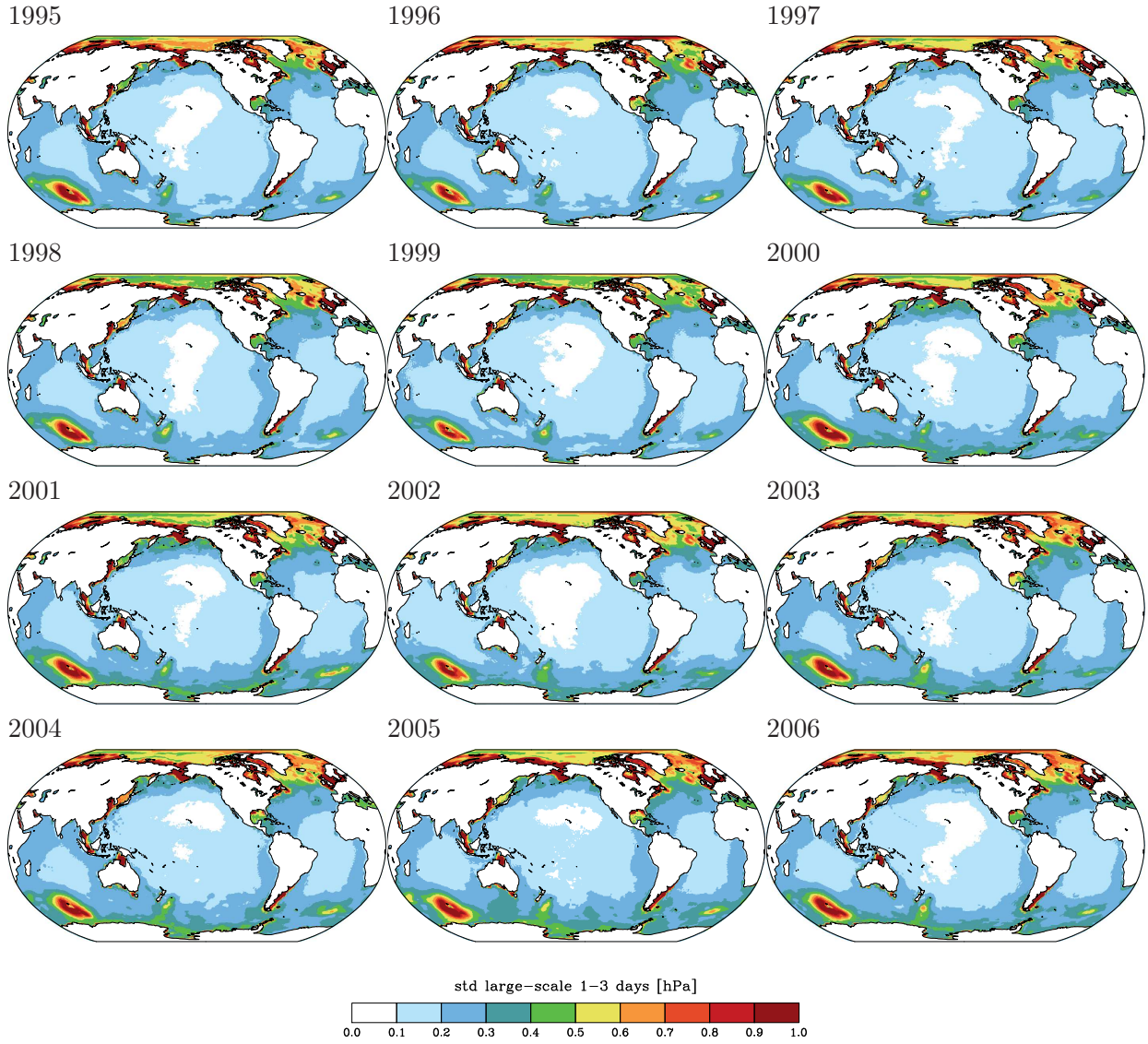

Figure 5.6: Rms of ocean bottom pressure errors with large spatial scales at periods of 1 – 3 days for individual years 1995 – 2006.

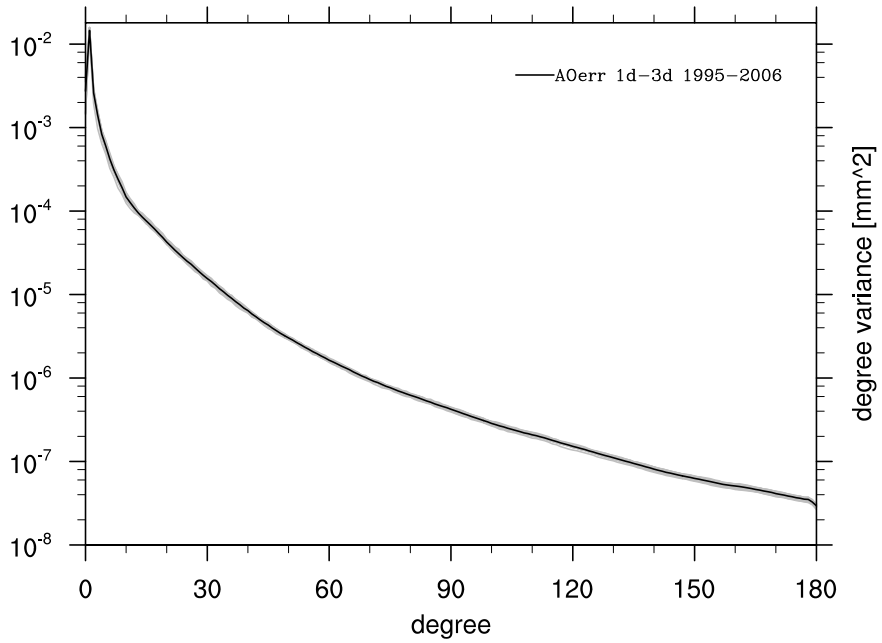

Figure 5.7: Degree variances for re-scaled large-scale true errors of atmosphere and ocean at periods of 1 – 3 days: averaged over 12 years (black) and for individual years 1995 – 2006 (grey).

Chapter 6

Errors with Large Spatial Scales at the S1 Frequency

6.1 Multi-Model Comparison for 2006

In contrast to the lunisolar gravitational tides, atmospheric tides or so-called air tides are predominantly caused by daily varying solar insolation, which is absorbed by water vapour and ozone in different height levels of the atmosphere. Changes in temperature and corresponding adjustments in the pressure and wind fields excite hemispheric waves that propagate laterally and horizontally, and thereby cause periodic variations at a given tidal frequency all around the globe.

In addition, tidal variations in atmospheric surface pressure cause periodic surface loads on the ocean surface that trigger also waves in the water at identical frequencies. Here, we treat atmospheric tides and their oceanic response in combination. Since air tides are principally caused by the diurnal cycle of the solar insolation, they occur at periods of 24 h and higher harmonics of it. Since the Nyquist period for a 6 hourly sampled dataset corresponds exactly to the period of the semi-diurnal air tide S2(p), it partially aliases into a standing wave pattern. Consequently, S2(p) signal parts are removed from the updated ESM, leaving only S1(p) tidal signals to be considered here.

From the 6 hourly ECMWF analyses, S1(p) is sampled at exactly the same phase every day. Its characteristics are therefore conveniently described by the mean tidal signal at the time-steps 00:00, 06:00, 12:00, and 18:00 h UTC. We calculate mean tidal signals for those time-steps from all four available atmospheric reanalyses and calculate pairwise rms model differences (Fig. 6.1). We find small-scale residual signals of 0.4 hPa in particular at tropical latitudes, where small-scale convective processes are of particular relevance for the S1(p) surface pressure signal. Largest differences are found between CFSR and MERRA over Africa, as well as between ERA-Interim and MERRA leewards of the Andes in South America. Based on those comparisons, we conclude that model differences between the original and the updated ESM scaled by 250% represents present-day uncertainities in the S1(p) in global atmospheric models fairly well.

Since ECCO2 and MPIOM STORM data are only available to us with a daily sampling, no information about the oceanic response to the atmospheric pressure tides is available for those models. Based on the comparison of OMCT and TUGO, we note large-scale differences of up to 1 hPa in all ocean basins apart from the Arctic, with a few localized peaks in some semi-enclosed seas as, for example, Gulf of Carpentaria and the Arafura Sea that even exceed this threshold (Fig. 6.3). Based on this comparison, we scale the differences between the original and the updated ESM by 150 % to arrive at a realistic representation of present-day errors in the S1 ocean tide (Fig. 6.4).

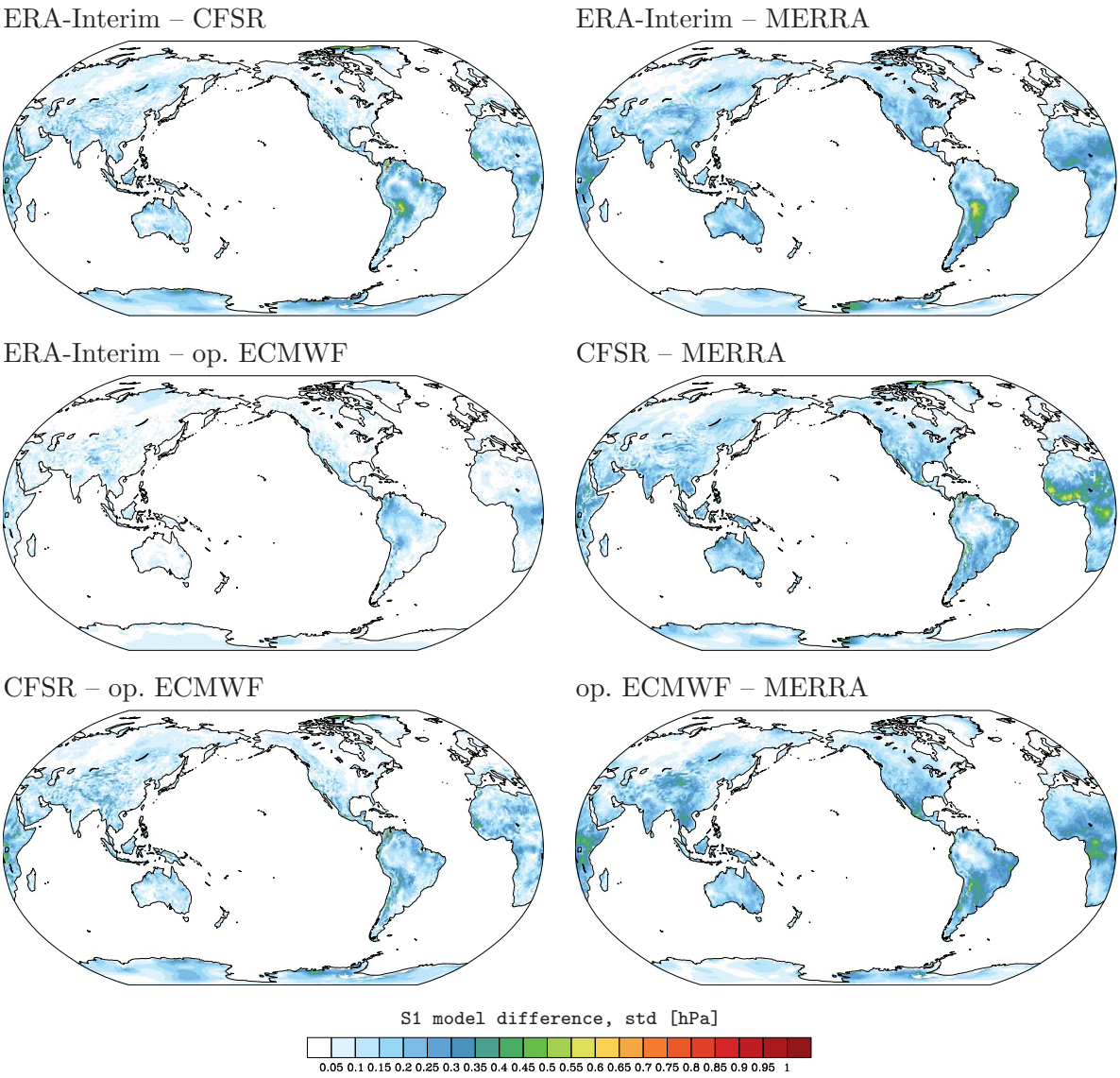

Figure 6.1: Rms differences of band-pass filtered atmospheric mass variability from four different global atmospheric surface pressure data-sets at the S1 period: ERA-Interim re-analysis, MERRA re-analysis, CFSR re-analysis, and ECMWF operational analyses.

6.2 Re-scaled Error Estimates for 1995 – 2006

Since mean S1 signals have been estimated for the 12 year period 1995 – 2006 from both the original and the updated ESM, the corresponding error derived from the re-scaled differences is consequently constant over the whole period both for the atmosphere (Fig. 6.5) and oceans (Fig. 6.6). Similarly, degree variances also do not reveal any deviations from year to year (Fig. 6.7).

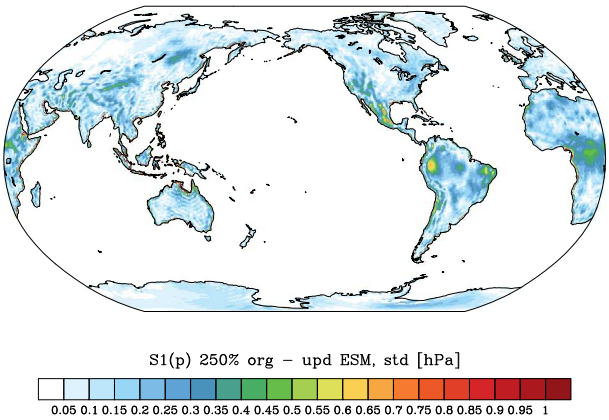

Figure 6.2: Rms differences of re-scaled atmospheric errors over the continents with large spatial scales at the S1 period as averaged over the period 1995 – 2006.

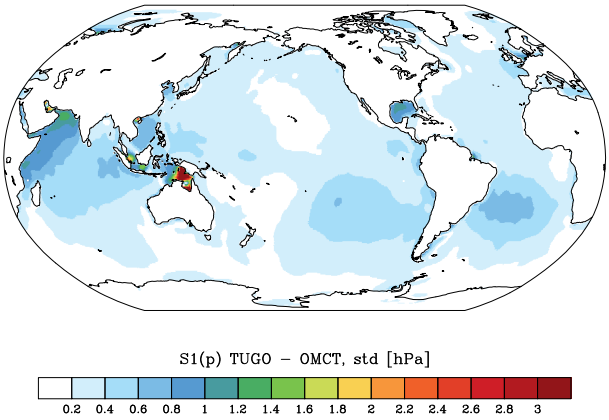

Figure 6.3: Rms differences of band-pass filtered ocean bottom pressure variability from two different global ocean bottom pressure data-sets at the S1 period: OMCT as used for AOD1B RL05 and TUGO.

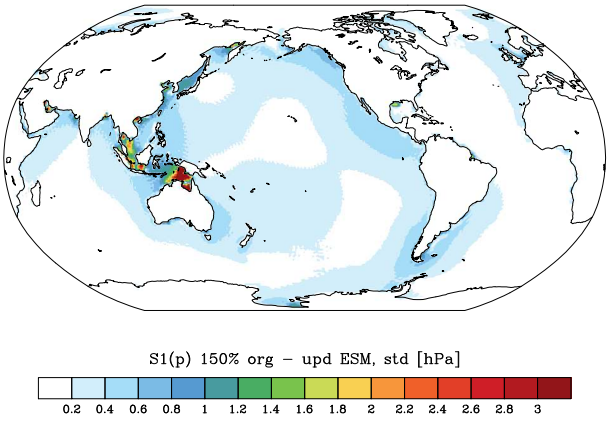

Figure 6.4: Rms differences of re-scaled ocean bottom pressure errors with large spatial scales at the S1 period as averaged over the period 1995 – 2006.

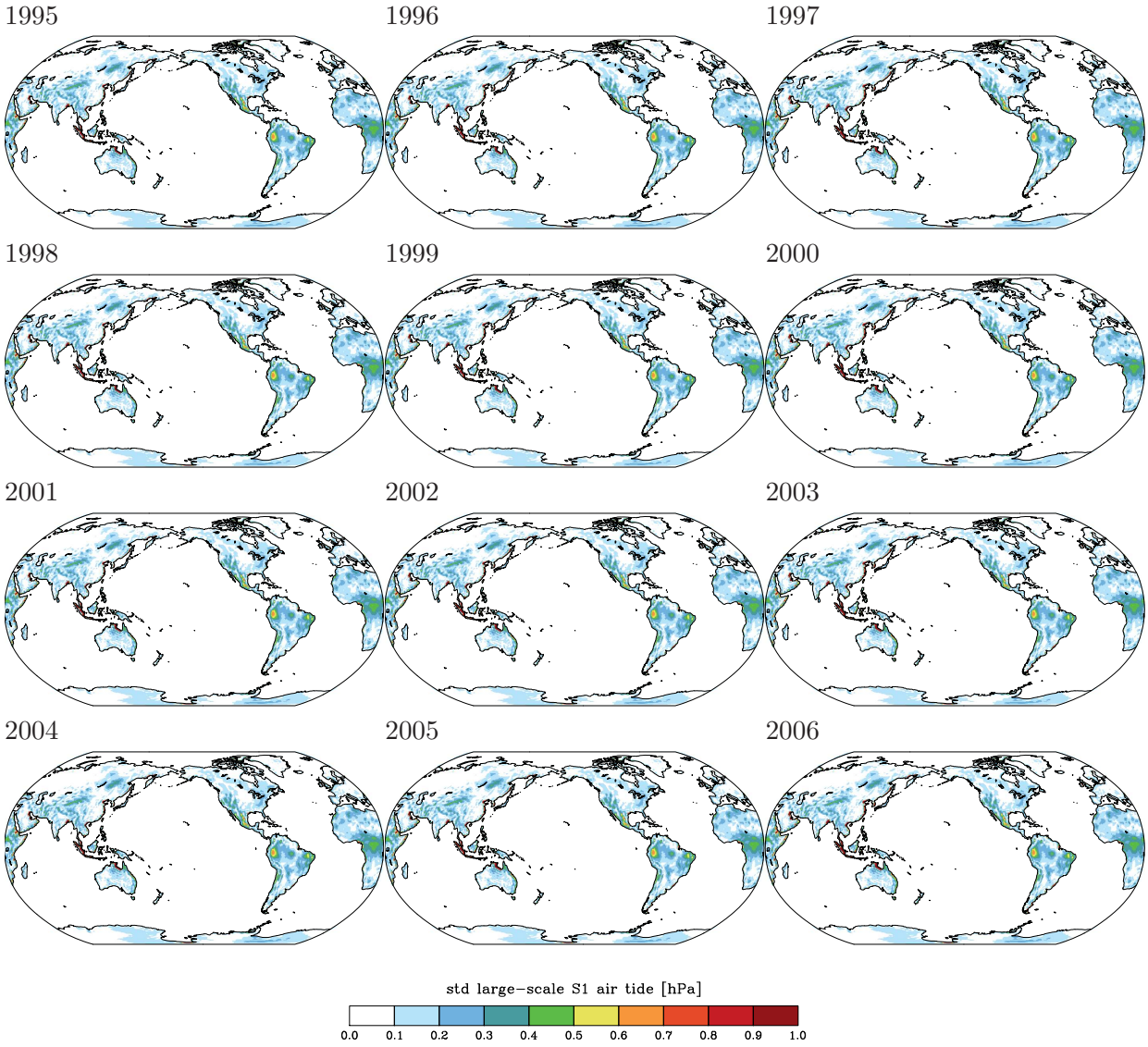

Figure 6.5: Rms of atmospheric errors with large spatial scales over the continents at the S1 period for individual years 1995 – 2006.

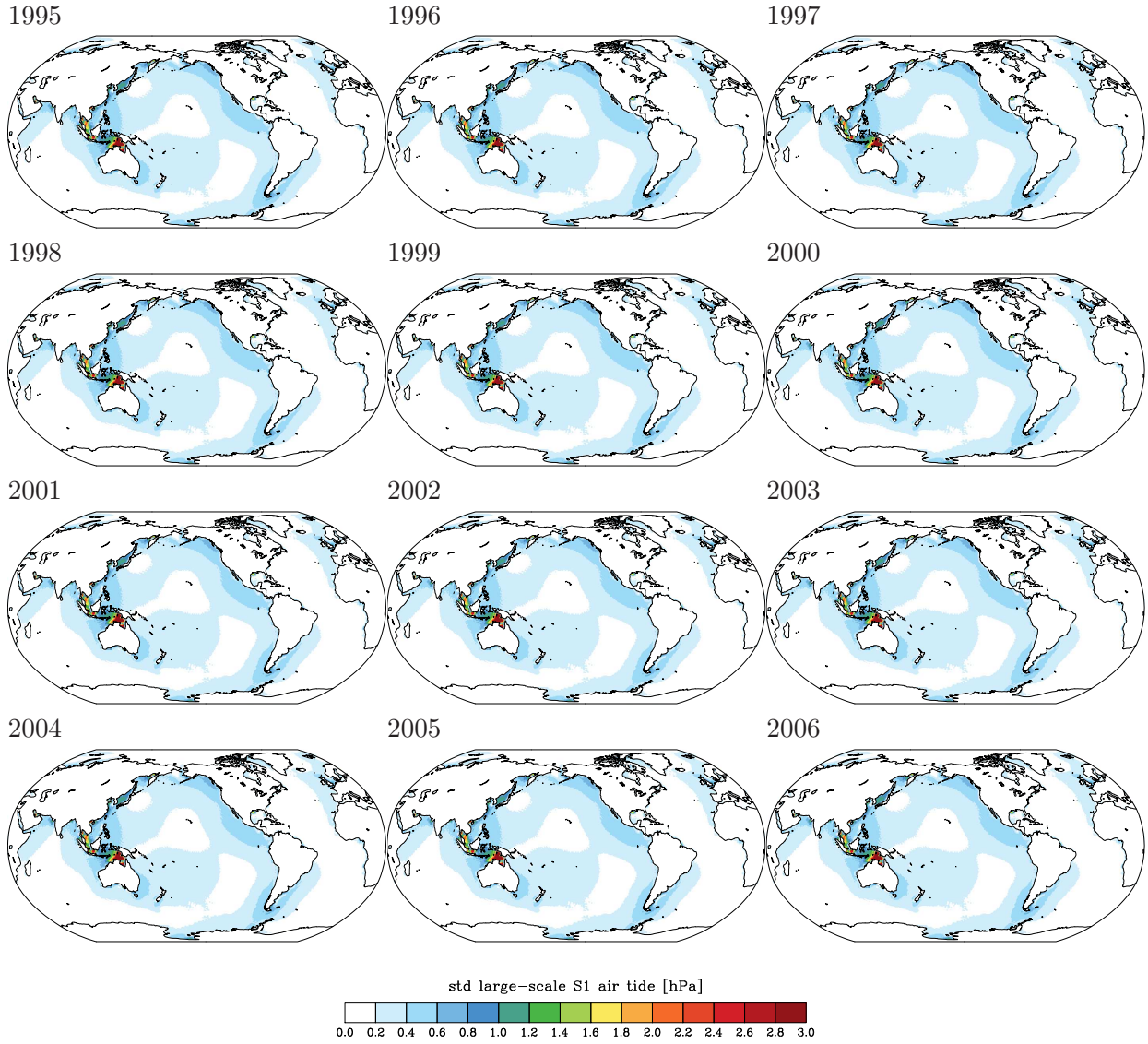

Figure 6.6: Rms of ocean bottom pressure errors with large spatial scales at the S1 period for individual years 1995 – 2006.

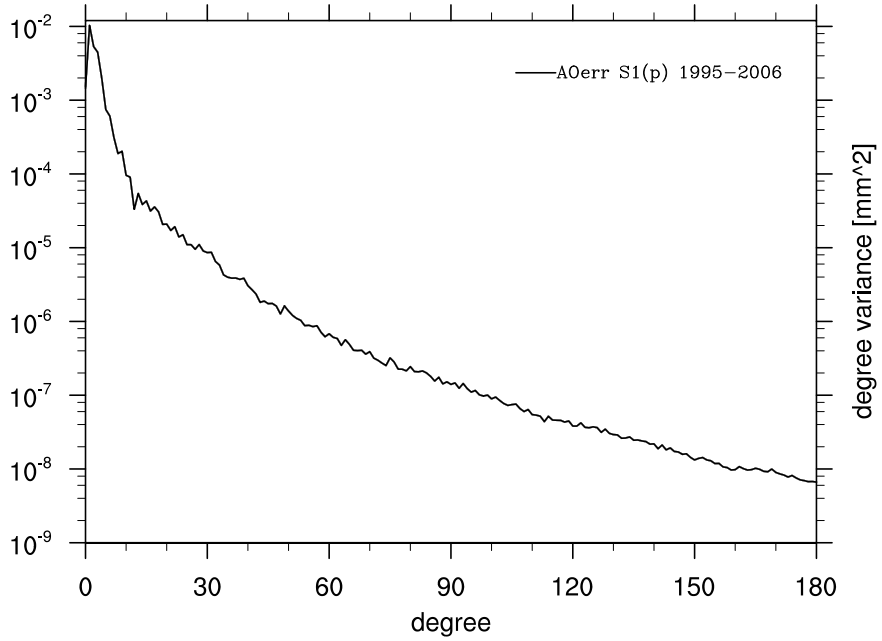

Figure 6.7: Degree variances for re-scaled large-scale true errors of atmosphere and ocean at the S1 period: averaged over 12 years (black). Individual years 1995 – 2006 are identical to the average over 12 years and consequently not shown.

Chapter 7

Errors with Large Spatial Scales at Sub-Diurnal Periods

7.1 Multi-Model Comparison for 2006

To focus on periods shorter than 24 hours, daily running mean values are subtracted from all four available atmospheric re-analysis datasets in order to retain only the signals at sub-diurnal frequencies only. Note that S1(p) and S2(p) signals averaged over the year 2006 are estimated and removed from each model prior to the comparison. Pairwise multi-model comparisons over the continents (Fig. 7.1) reveal residual signals of 0.4 hPa globally that extend up to 1 hPa in coastal regions of Antarctica.

So far, the assessment of all error components has been based on 6 hourly sampled data only, consistent with the sampling of the original and the updated ESM. Global atmospheric datasets are available to us at 3 hourly (ERA-Interim) or even hourly (CFSR and MERRA) intervals. To assess the variability that is potentially missed out from 6 hourly data, we sub-sample the datasets to 6 hourly resolution, interpolate back linearly between the 6 hourly time-steps to the original temporal resolution and calculate standard deviations between the original and the interpolated model time-series (Fig. 7.2).

Since errors at periods associated with a temporal sampling shorter than 6 hours are not explicitly reproducible by the error model prepared in this study, we decide to upscale the 6 hourly sampled error series to also account for this contribution in its overall level of variability. We therefore scale the 6 hourly sub-daily model differences between the original and the updated ESM by 180 % (Fig. 7.3).

For the oceans, we calculate sub-daily model differences in ocean bottom pressure between TUGO and OMCT (Fig. 7.4). Basin-wide signals have a typical magnitude of 0.8 hPa, with even stronger but rather localized peaks in several semi-enclosed basins that reach up to 3 hPa. In addition, variability at periods not covered by a 6 hourly sampled dataset (Fig. 7.5) adds about 0.5 hPa variability on top of the signals discussed before. We therefore conclude that it is reasonable to scale the sub-diurnal model differences between the original and the updated ESM by 150 % for the oceanic areas (Fig. 7.6).

7.2 Re-scaled Error Estimates for 1995 – 2006

Model differences at sub-diurnal periods that are re-scaled with individual constants for atmosphere and oceans are analyzed up to d/o = 180 for all 12 years. Subsequently, coefficients are re-

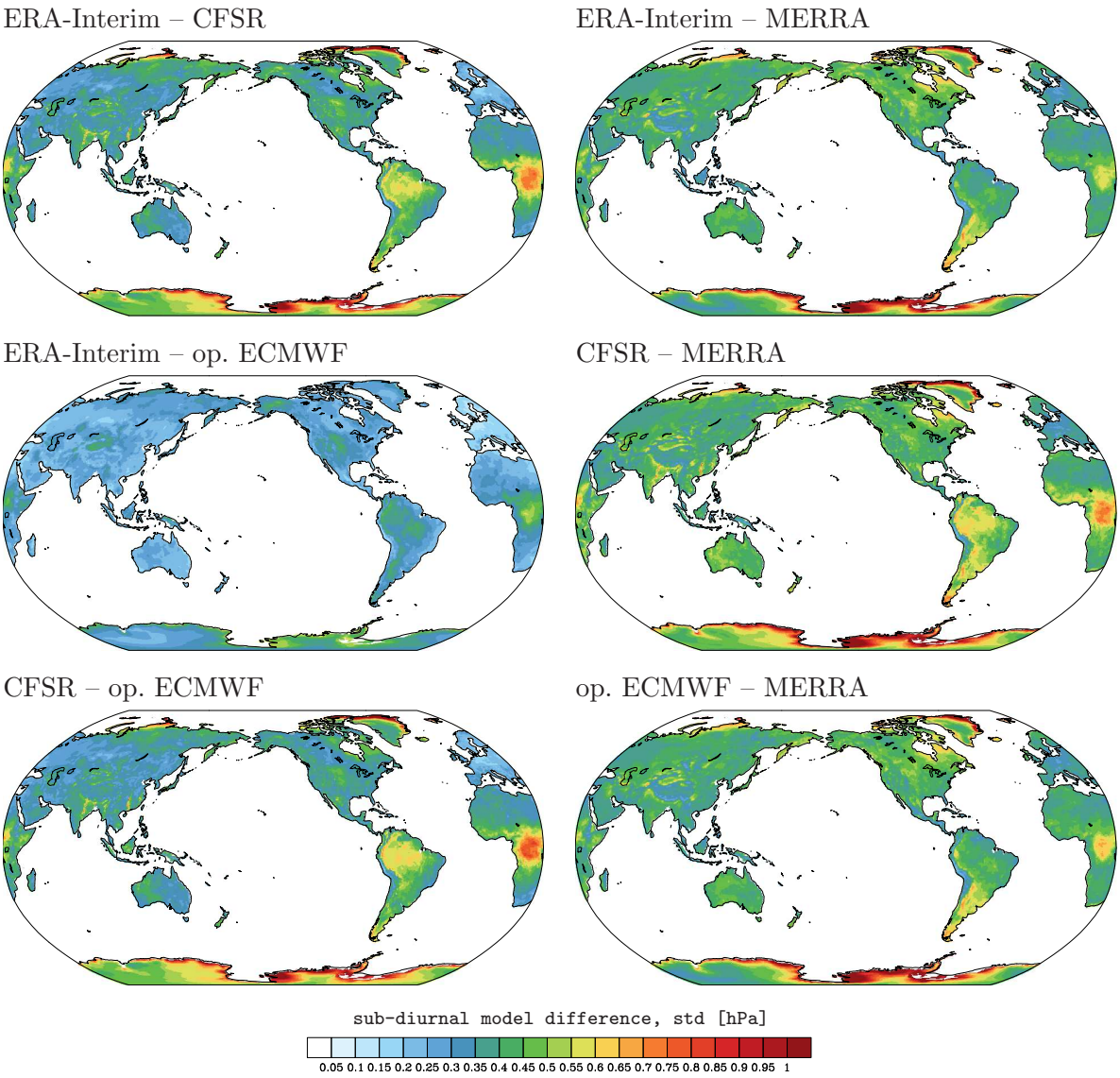

Figure 7.1: Rms differences of band-pass filtered atmospheric mass variability from four different global atmospheric surface pressure data-sets at sub-diurnal periods: ERA-Interim re-analysis, MERRA re-analysis, CFSR re-analysis, and ECMWF operational analyses.

synthesized onto the original 0.5° grid and standard deviations for all individual years are calculated. For the atmosphere, we note weak non-stationarities reflecting changes in the operational ECMWF and ERA-40 datasets during various years (Fig. 7.7). For the oceans, we note stronger year-to-year variability with some exceptional features in the Southern Ocean in 2005 (Fig. 7.8). Degree variances of the combined atmosphere and ocean variability, however, do not reveal substantial differences among the individual years (Fig. 7.9).

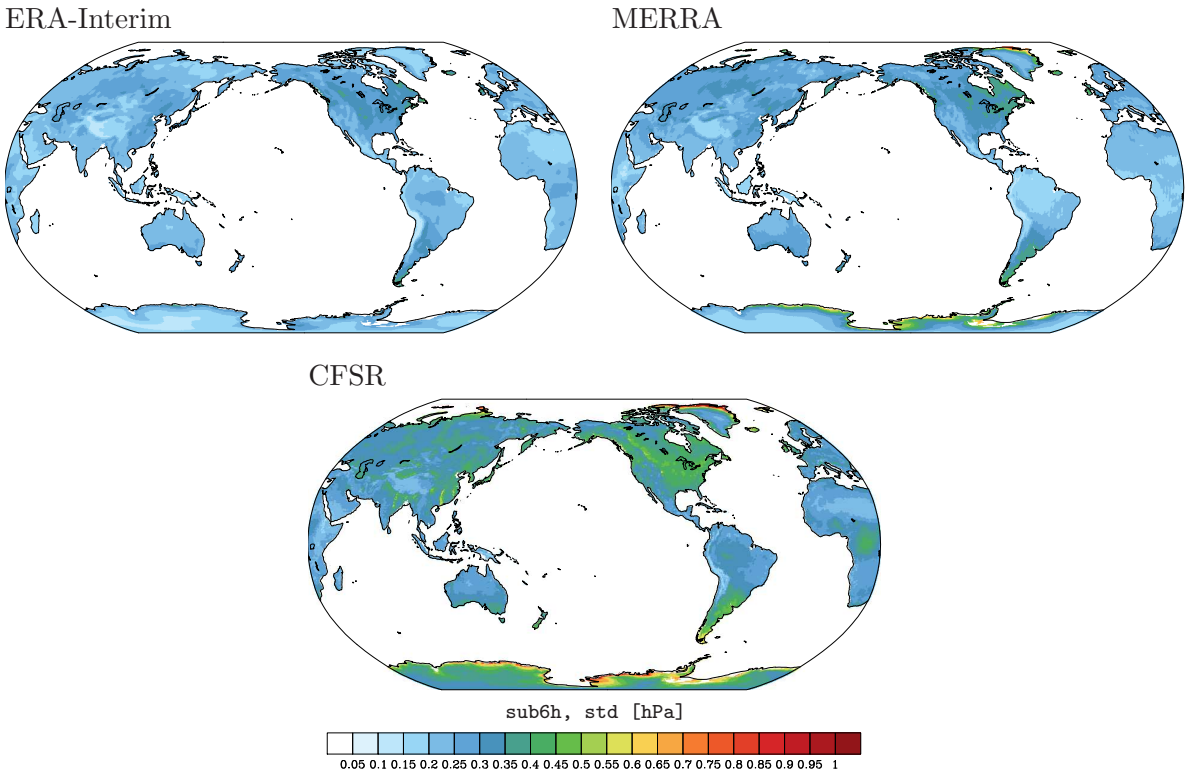

Figure 7.2: Rms of high-pass filtered atmospheric surface pressure anomalies from three different global atmospheric data-sets at periods shorter than 6 hours: ERA-Interim re-analysis, MERRA re-analysis, and CFSR re-analysis.

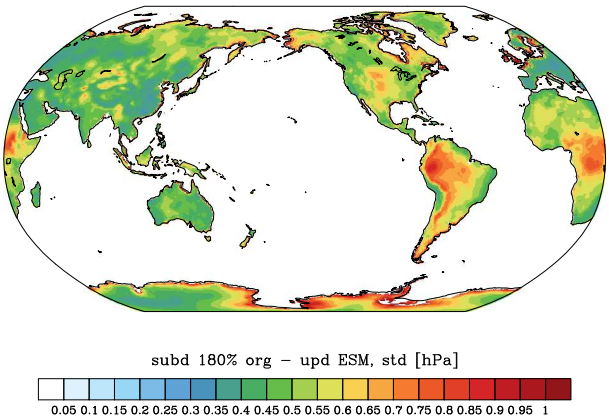

Figure 7.3: Rms differences of re-scaled atmospheric errors over the continents with large spatial scales at sub-diurnal periods as averaged over the period 1995 – 2006.

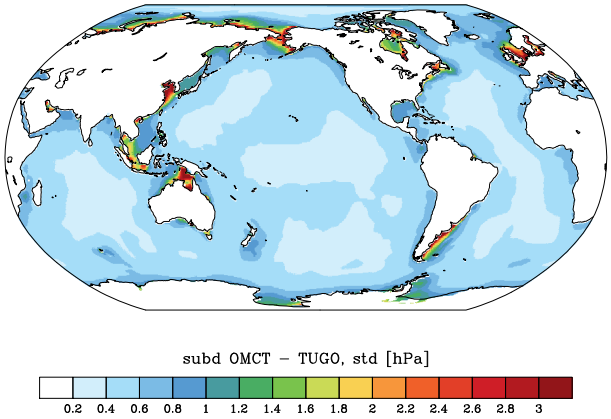

Figure 7.4: Rms differences of band-pass filtered ocean bottom pressure variability from two different global ocean bottom pressure data-sets at sub-diurnal periods: OMCT as used for AOD1B RL05 and TUGO.

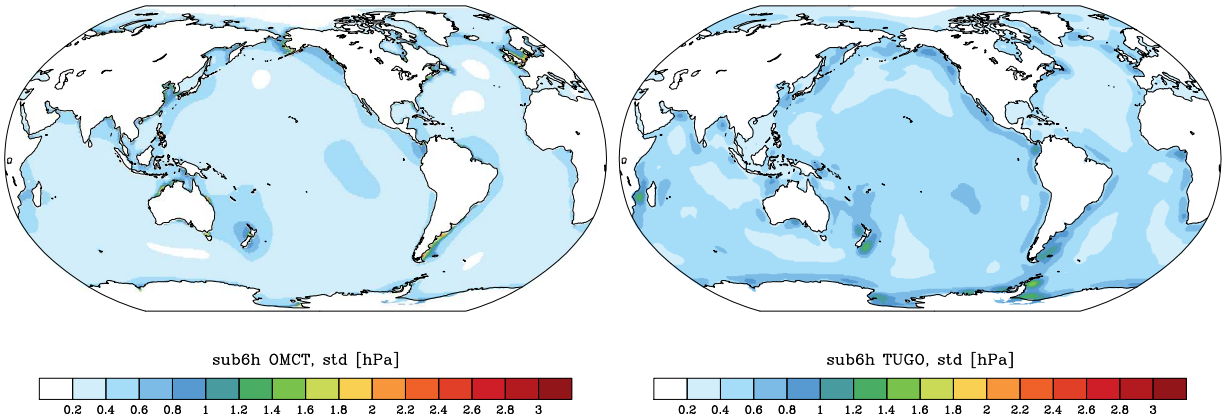

Figure 7.5: Rms differences of high-pass filtered ocean bottom pressure variability from two different global ocean bottom pressure data-sets at periods shorter than 6 hours: OMCT as used for AOD1B RL05 and TUGO.

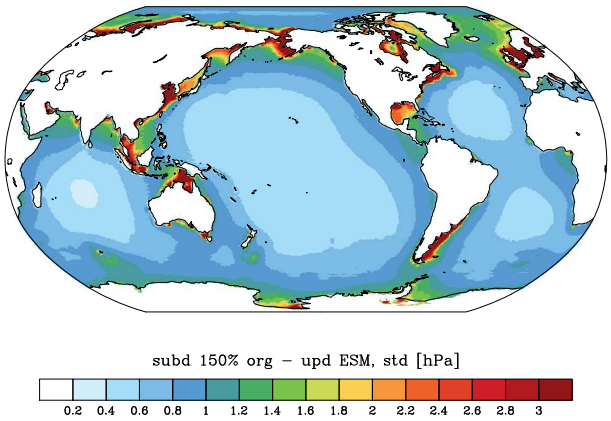

Figure 7.6: Rms differences of re-scaled ocean bottom pressure errors with large spatial scales at sub-diurnal periods as averaged over the period 1995 – 2006.

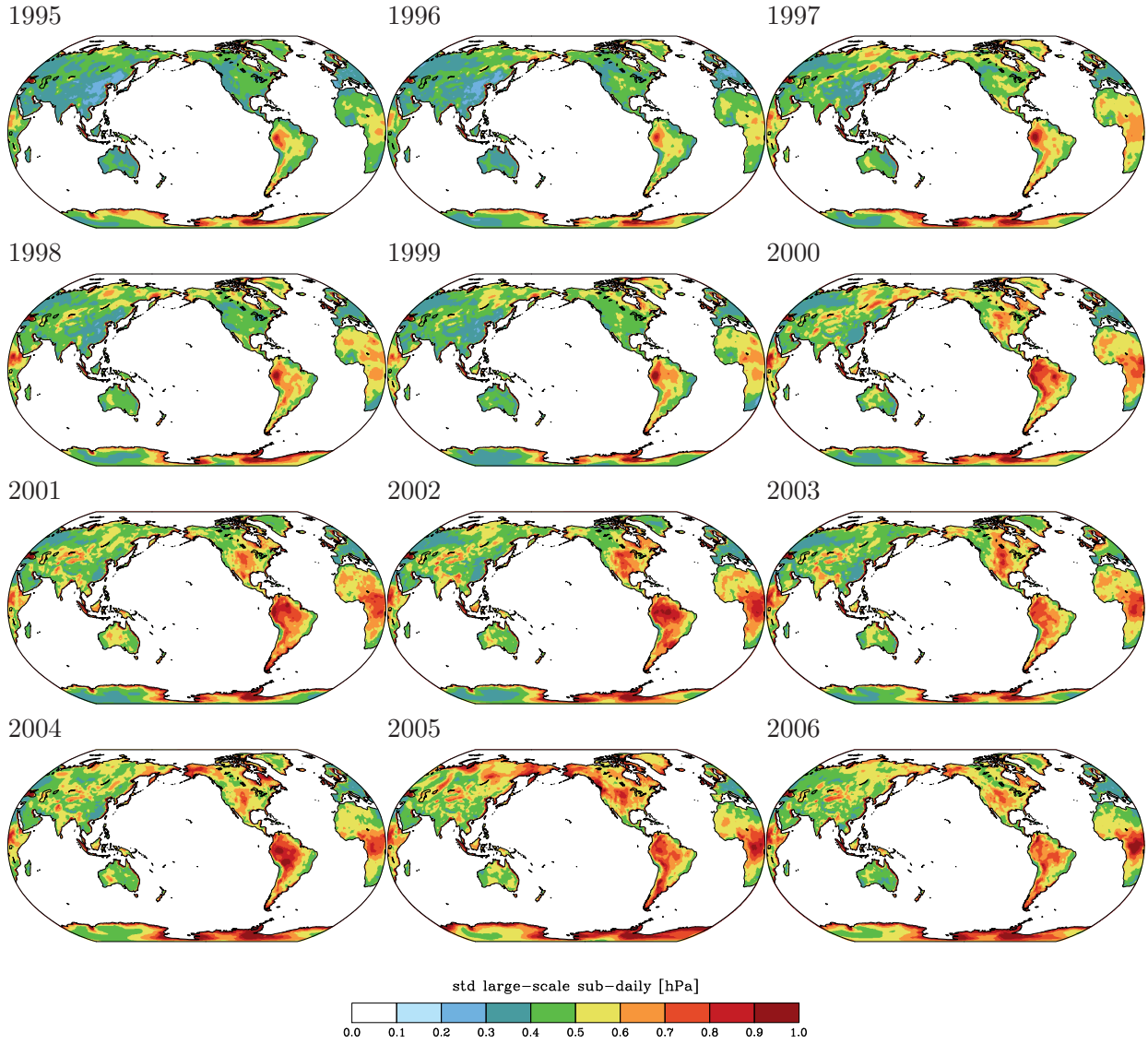

Figure 7.7: Rms of atmospheric errors with large spatial scales over the continents at sub-diurnal periods for individual years 1995 – 2006.

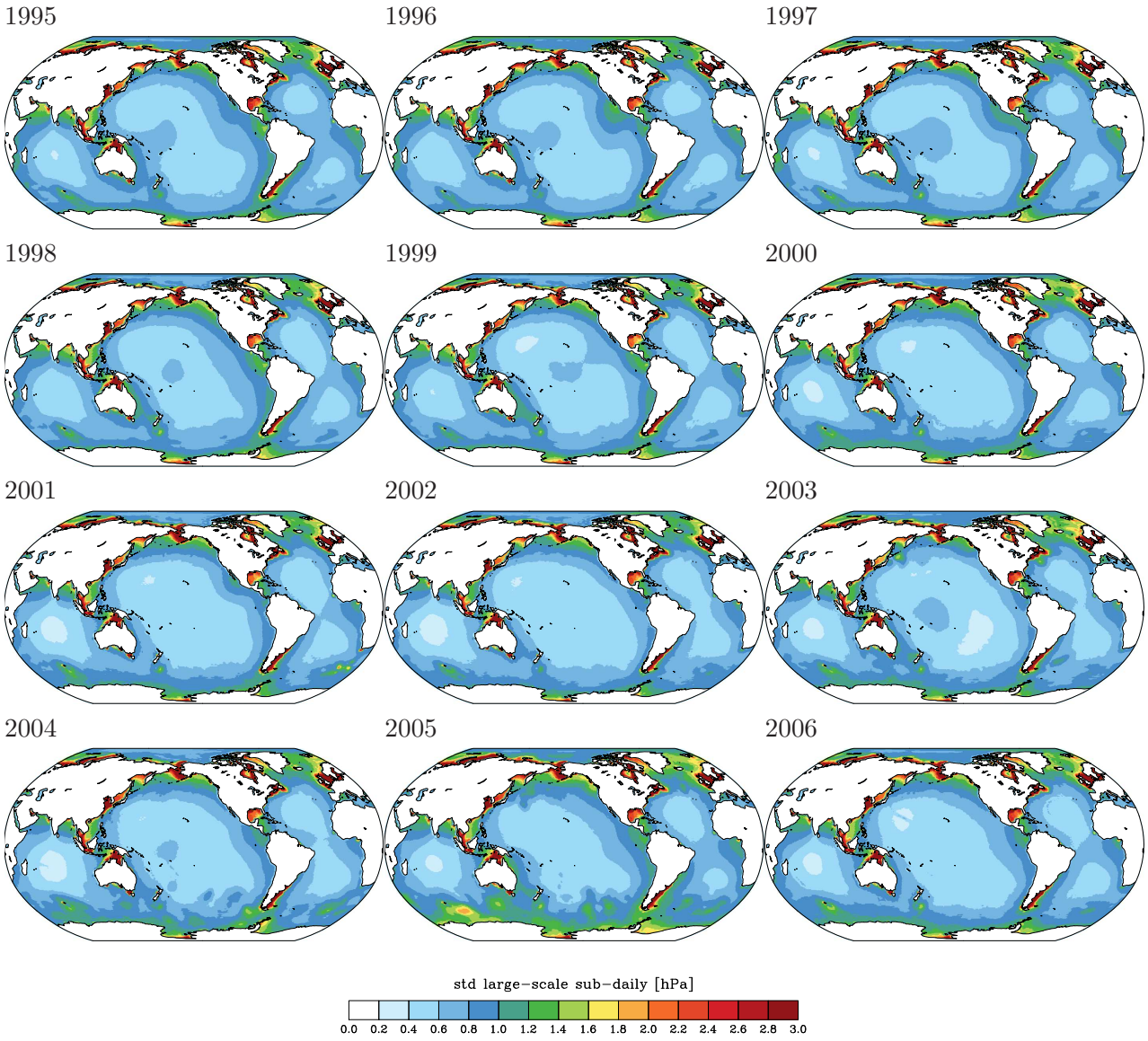

Figure 7.8: Rms of ocean bottom pressure errors with large spatial scales at sub-diurnal periods for individual years 1995 – 2006.

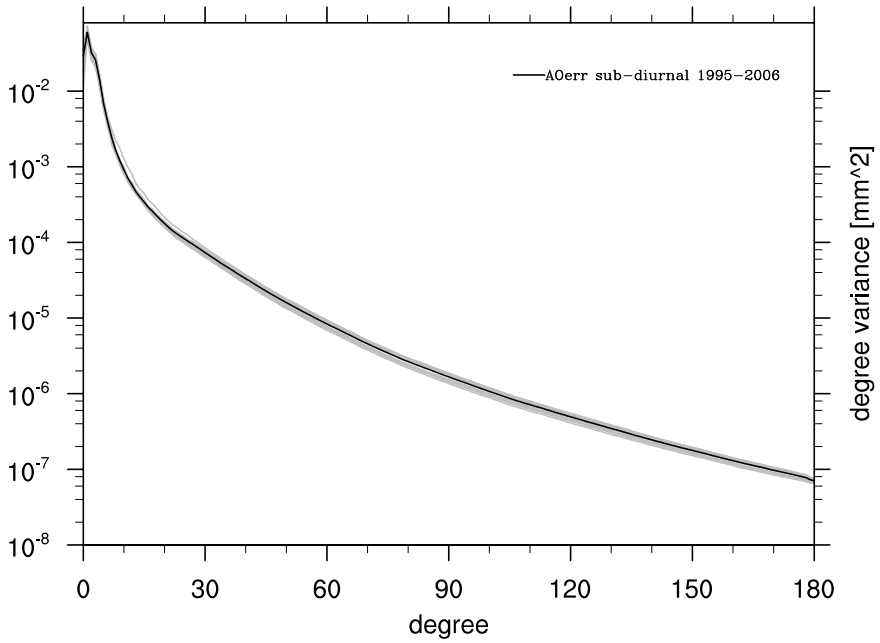

Figure 7.9: Degree variances for re-scaled large-scale true errors of atmosphere and ocean at sub-diurnal periods: averaged over 12 years (black) and for individual years 1995 – 2006 (grey).

Chapter 8

Errors at Small Spatial Scales as Approximated From a Regional Model

8.1 High-Resolution Regional Atmospheric Model Data from COSMO-EU

Global atmospheric re-analyses are confined to the representation of the atmospheric dynamics, land-surface interactions, and orographic effects at large spatial scales, since the discretization of the model equations in time and space requires the parametrization of local processes from a certain scale on. The updated ESM over its full 12 year period is available in spherical harmonic coefficients up to d/o = 180, which roughly corresponds to a spatial resolution of 1°. In reality, there is certainly variability at spatial scales below that threshold that might potentially leak into degrees and orders smaller than 180.

To assess signals at small spatial scales not covered explicitly by the updated ESM, we utilize data from a recent experiment with the non-hydrostatic very high-resolution numerical weather prediction model COSMO-EU (Baldauf *et al.*, 2011). The model is discretized over the European CORDEX domain with a horizontal resolution of approximately 7 km. Available to us are data for the year 2006 from an operational analysis run with a temporal sampling of 3 hours. To isolate

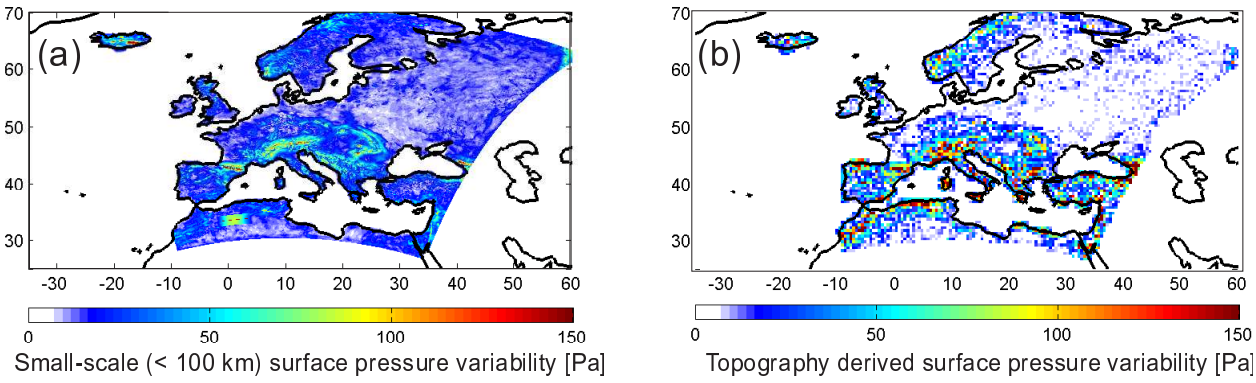

Figure 8.1: Rms of the pressure signals at small spatial scales that are typically missed out by global atmospheric data-sets (a) and reconstruction of small-scale atmospheric errors based on the local topographic roughness (b) over the COSMO-EU model domain.

small-scale signals at the periods in question, a high-pass filter with 30 days cutoff period is applied to the surface pressure anomalies. Subsequently, 1° spatial averages are removed from the high-pass filtered pressure anomalies to arrive at anomalies at spatial scales smaller than approximately 100 km.

Standard deviations of residual pressure signals at small spatial scales reveal signals of up to 1.5 hPa in mountaineous regions as, for example, the Alps and the Pyrenees (Fig. 8.1a). Those signals are highly localized and in particular confined to areas with very rough topography. Most other regions, instead, show residual pressure signals that are well below 0.5 hPa.

8.2 Approximation of Global Small-Scale Error Estimates from Regional Data

Since high-resolution model data is only available to us from an atmospheric model on the European continent, we need to find a way to extrapolate those errors to the globe. For this, we hypothesize a linear relationship between the roughness of the topography and residual pressure signals at small spatial scales. By doing so, a global topographic dataset that also includes sub-surface bathymetry over the oceans as ETOPO2 is a suitable predictor for a linear regression model to be set-up over the COSMO-EU model domain.

To obtain a roughness scale, we smooth ETOPO2 topography at its original grid with a spatial resolution of 2′ by a two-dimensional moving average filter with a window lenghth of 30 grid cells, which roughly corresponds to a 1° spatial resolution. The difference between the original topography and the smoothed version is taken as topographic roughness indicator for the regression model. We find that small-scale pressure variability as obtained from topographic roughness based on ETOPO2 and the regression model at a 0.5° spatial resolution approximates the signal quite well (Fig. 8.1b).

8.3 Re-scaled Error Estimates for 1995 – 2006

Based on the variability of surface and bottom pressure errors at small spatial scales predicted from the regression model, we randomly sample errors from zero-centered normal distributions with the given variances in order to arrive at 250 indepent global realizations of small-scale model differences. By doing so, we implicitly assume that the errors are (i) uncorrelated in space – which is certainly justified by the fact that we are only concerned with residual signals at spatial scales below the grid-scale considered – and (ii) uncorrelated in time, which is certainly only true for periods longer than a few hours. We account for this fact by treating the 250 realizations as daily estimates that are subsequently linearly interpolated to a temporal sampling of 6 hours. To cover the full period of 12 years, the 250 daily realizations are cycled for about 18 times. The number of 250 realizations has been chosen somewhat arbitrarily in order to avoid from the very beginning any interference with geophysically relevant frequencies as, e.g., the seasonal cycle or quasi-periodic phenomena as the quasi-biennial oscillation in the Atmosphere, the El Nino Southern Oscillation of the climate system, or the Solar Cycle.

Small-scale errors expanded into spherical harmonics up to d/o = 180 for every 6 hours are synthesized back onto a 0.5° grid to calculate standard deviations for continental (Fig. 8.2) and oceanic (Fig. 8.3) regions for each year of the period 1995 to 2006. Since all errors are derived from 250 daily realizations only, estimates are stationary for all years considered, and degree variances (Fig. 8.4) for all years do not show systematic differences. We note that signal magnitudes predicted from the regression model over the oceans are larger than over land by approximately a factor of two, which

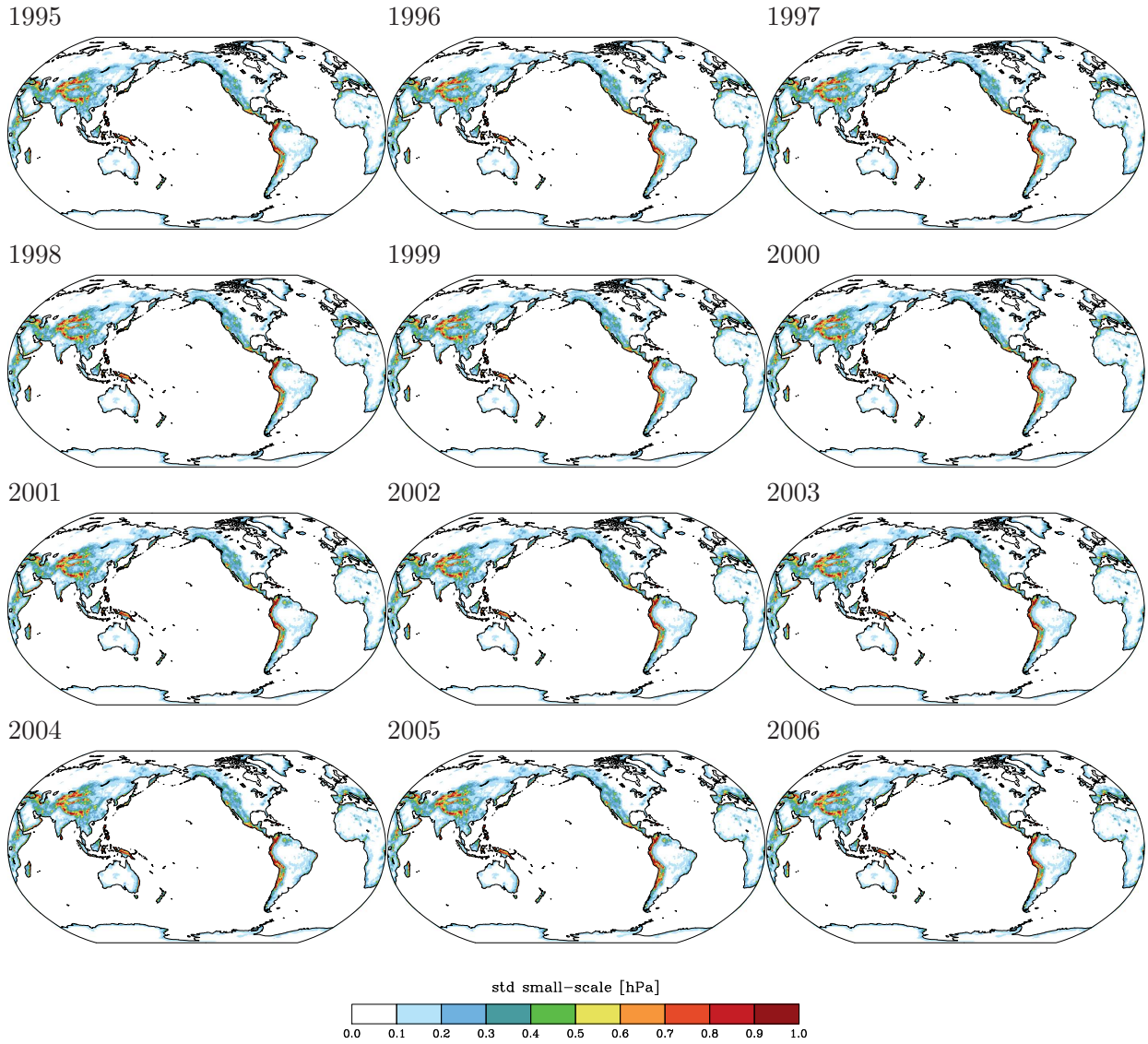

Figure 8.2: Rms of atmospheric errors with small spatial scales over the continents for individual years 1995 – 2006.

is related to the steep sub-surface bathymetric changes in particular around deep sea trenches. Based on our previous experience that ocean bottom pressure errors are typically larger than those of continental signals at similar frequencies, we believe that this magnitude of oceanic small-scale errors is certainly not overly pessimistic.

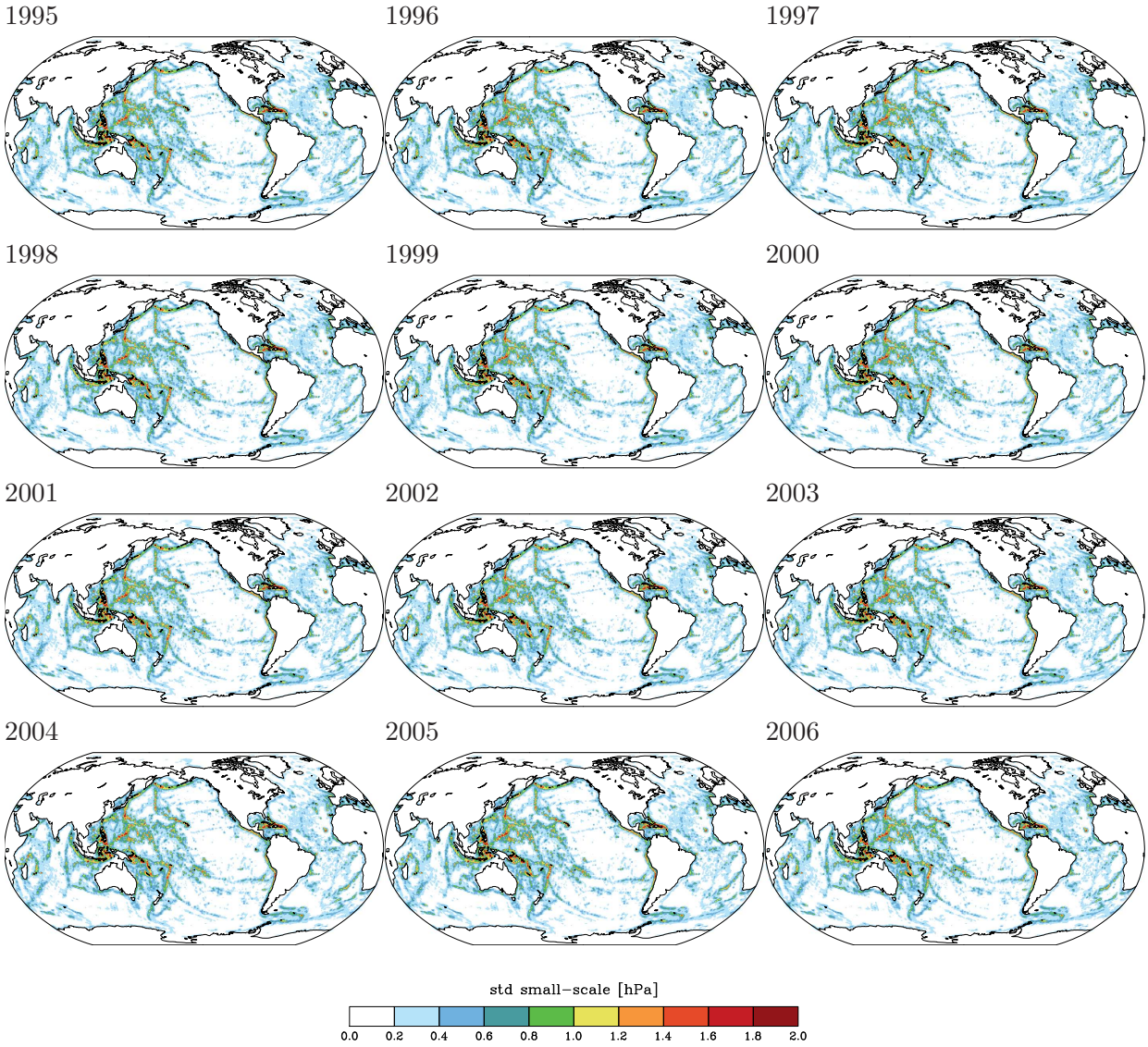

Figure 8.3: Rms of ocean bottom pressure errors with small spatial scales for individual years 1995 – 2006.

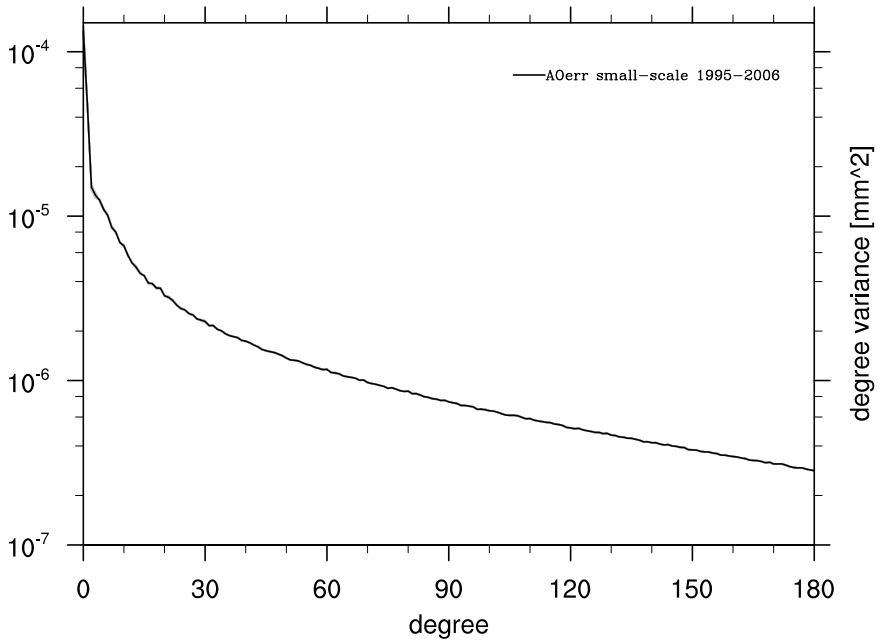

Figure 8.4: Degree variances for small-scale true errors of atmosphere and ocean: averaged over 12 years (black). Individual years 1995 – 2006 are identical to the average over 12 years and consequently not shown.

Chapter 9

Summary

9.1 Characteristics of the Perturbed De-Aliasing Model

The realistically perturbed de-aliasing model that is consistent with the updated ESA Earth System Model (Dobslaw *et al.*, 2015) consists of two sets of spherical harmonic coefficients: First, an unperturbed de-aliasing model of non-tidal mass variability in atmosphere and ocean ('DEAL' coefficients), and secondly, a series of true errors ('AOerr' coefficients). Both data-sets need to arrive at a realistically perturbed de-aliasing model in order to reproduce realistic aliasing errors in a satellite mission simulation environment.

The characteristics of the error model averaged over 1995 – 2006 are summarized in Fig. 9.1. It consists of large-scale errors at different frequency bands and an estimate of the small-scale error variability derived from the local roughness of the topography. For the atmosphere, we note fairly homogeneous errors at large spatial scales for all frequency bands considered. For the oceans, we find a clear latitude dependence with almost no error in the tropics and peak values in the west wind regime at moderate to high extra-tropical latitudes. In addition, we note that different subsurface ocean basins have different resonance frequencies that lead to peak error levels in different sectors of the southern ocean for different period bands considered. Together with the errors due to physical processes in the ocean that are intentionally omitted from the de-aliasing model, those in total six error components form the complete error model of the realistically perturbed de-aliasing model that is consistent with the updated ESA ESM.

For completeness, the individual error components are also expressed in terms of degree variances (Fig. 9.2). We note that individual error components cause variability that is well below the signal degree variance of atmospheric and oceanic mass variability. The relative level of the error components depends highly on the spectral width of the band-pass filters applied and is thus somewhat arbitrary. It is, however, interesting to see that sub-daily variability has higher energy in the spectral band $40 \leq d \leq 70$ compared to the slower processes. Moreover, we find that the combined errors are larger than the signals for degrees higher than 60. Since those signals are, nevertheless, dominated by rather slowly evolving processes as discussed in Ch. 2, they contribute to the actual aliasing errors by a small fraction only.

9.2 Atmospheric and Oceanic Variability of the updated ESA ESM as Explained by the Perturbed De-Aliasing Model

In order to contrast the error model to the actual signals of non-tidal mass variability in atmosphere and oceans, we assess how much variance of the A and O components of the source model are

finally explained by the realistically perturbed de-aliasing model. When focusing on unfiltered data (Fig. 9.3), highest absolute explained variances are found on land at extra-tropical latitudes, where the strongest signals with large seasonal variations reside. Relative explained variances over the continents are close to 100%, only around the equator – where atmospheric tides dominate even long-term pressure records – we note lower relative explained variances down to 50 %. For the oceans, absolute explained variances are substantially lower due to both, the lower signal magnitudes and the higher error levels. Relative explained variances hardly exceed 80 % and are in particular low in the Arctic Ocean, and in the northern and tropical Atlantic.

This picture changes slightly when both the atmospheric and oceanic signals and the perturbed de-aliasing model are high-pass filtered for periods shorter than 30 days with a 3rd order butterworth filter (Fig. 9.4). Over the continents, the perturbed de-aliasing model still explains a major fraction of the signal. The only exception are the tropical latitudes dominated by the atmospheric tides, as, for example, in Ecuador in South America, where basically nothing of the signal is explained. For the oceans, the performance of the model is even worse, showing relative explained variances of more than 60 % only in some isolated sub-surface basins in the southern ocean, and – albeit at a lower level of around 50 % – also in the North Pacific and the North Atlantic. Large regions around the continents, however, reveal no skill at all, and also the Arctic Ocean variability is once more rather poorly predicted by the perturbed de-aliasing model.

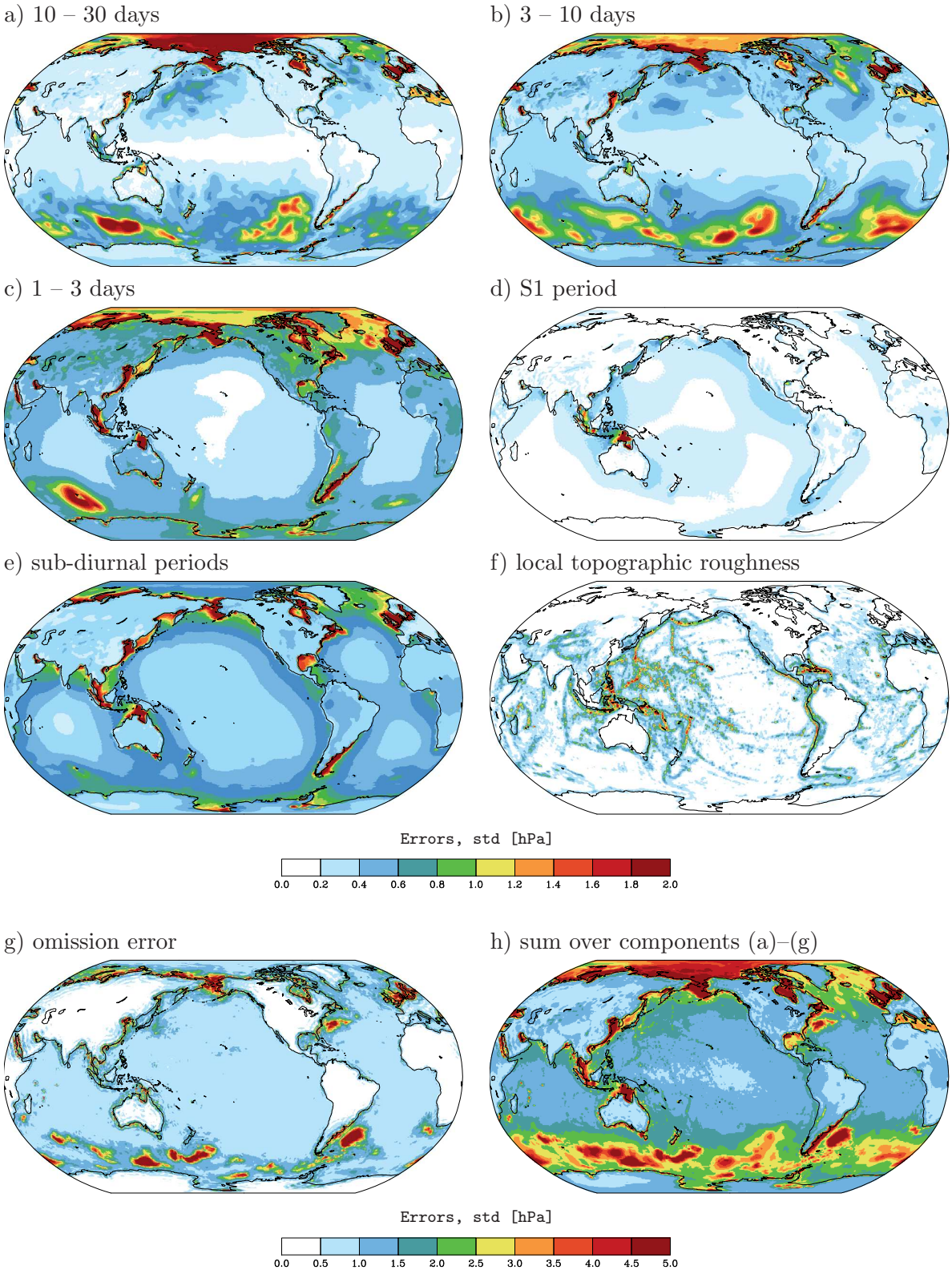

Figure 9.1: Rms variability of all components of the realistically perturbed de-aliasing model: (a)–(e) large scale errors at different periods; (f) small-scale errors derived from the local topographic roughness; (g) errors due to physical processes not included into GRACE AOD1B; and (h) sum over all components of the perturbed de-aliasing model.

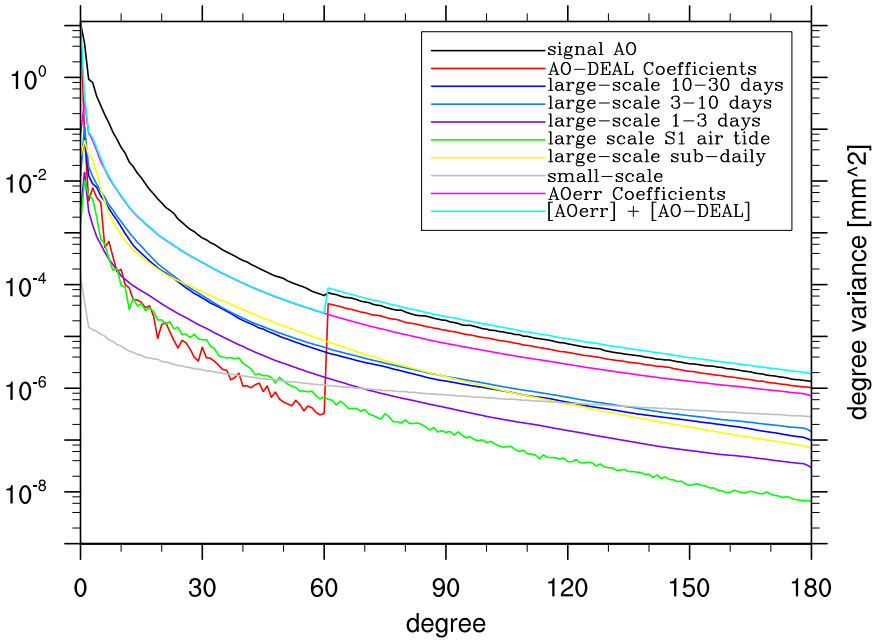

Figure 9.2: Degree variances for all individual error model compoents and the summarized model as averaged over 12 years.

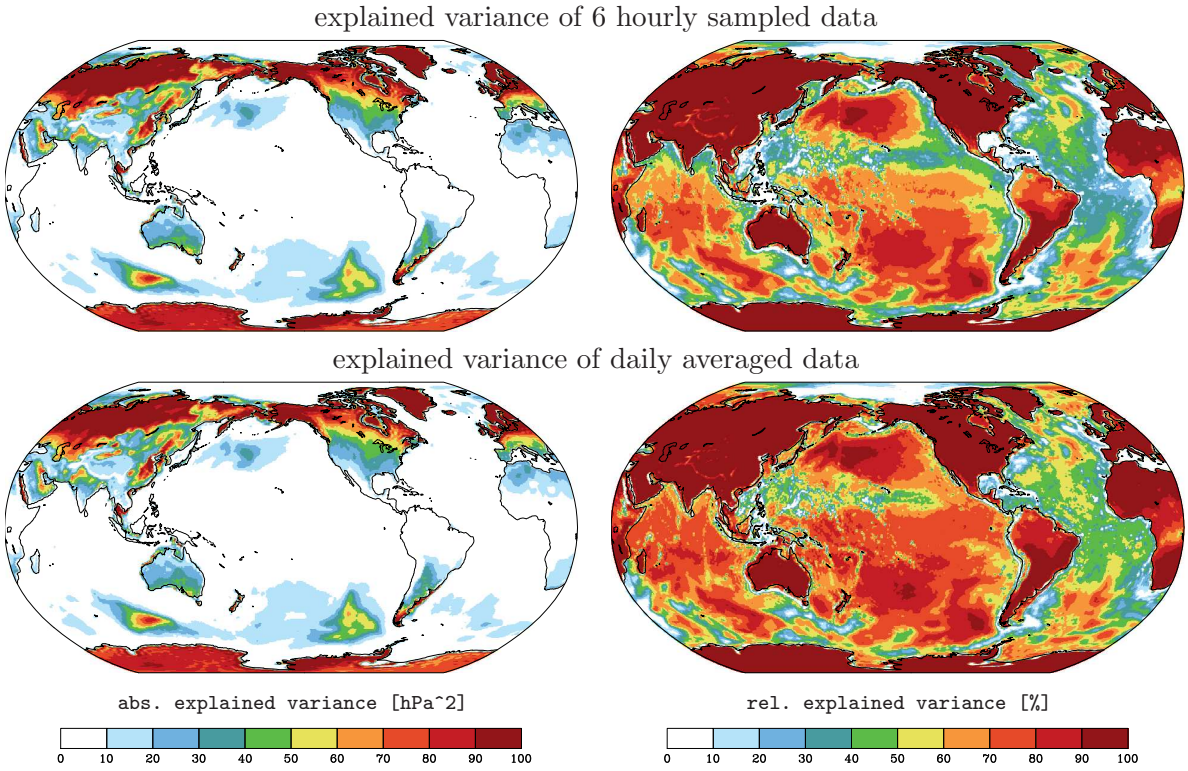

Figure 9.3: Absolute (left) and relative (right) variance of the AO component of the updated ESM explained by the realistically perturbed de-aliasing model: 6 hourly sampled data (top row), and daily averaged data (bottom row).

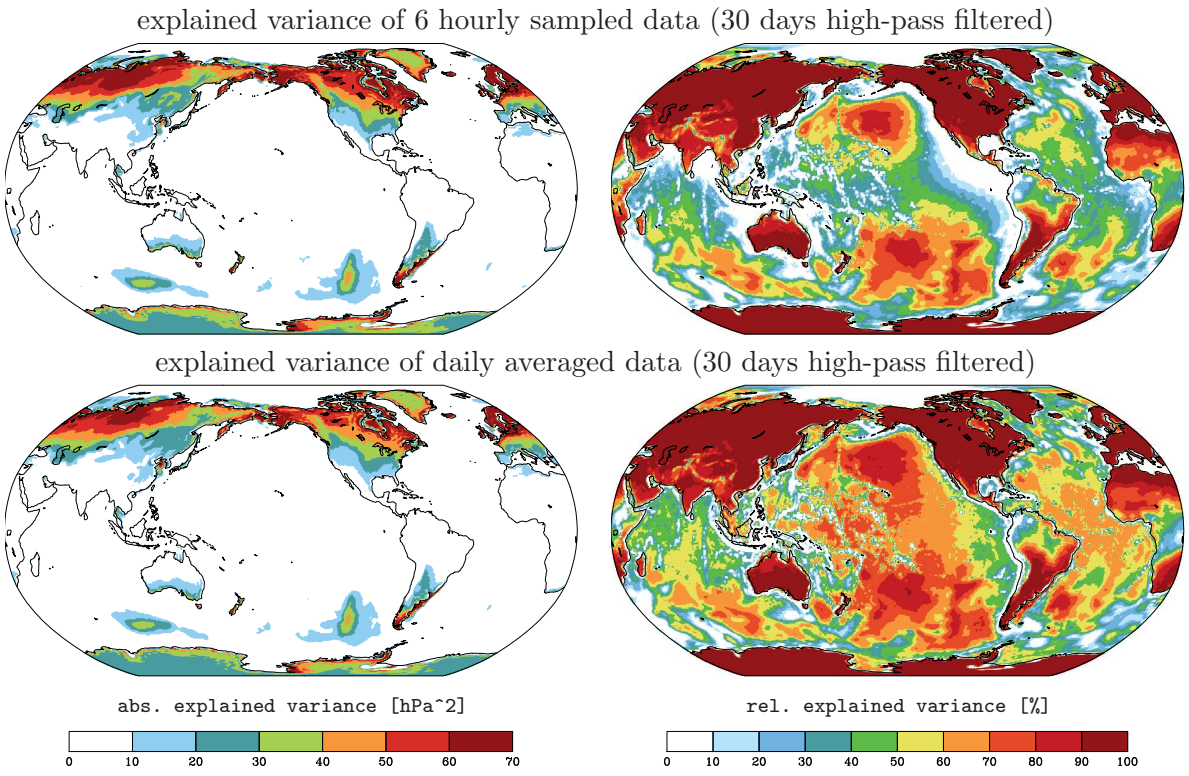

Figure 9.4: Absolute (left) and relative (right) variance of the AO component of the updated ESM explained by the realistically perturbed de-aliasing model that are both filterred with a 30 days high-pass filter: 6 hourly sampled data (top row), and daily averaged data (bottom row).

Bibliography

Baldauf, M., Seifert, A., Förstner, J., Majewski, D., Raschendorfer, M. & Reinhardt, T. (2011). Operational Convective-Scale Numerical Weather Prediction with the COSMO Model: Description and Sensitivities, *Mon. Weather Rev.*, **139**, 3887–3905, doi:10.1175/MWR-D-10-05013.1. 49

Bergmann-Wolf, I., Dill, R., Forootan, E., Klemann, V., Kusche, J., Sasgen, I. & Dobslaw, H. (2014). *Updating ESA's Earth System Model for Gravity Mission Simulation Studies: 2. Comparison with the Original Model*, *Tech. rep.*, Scientific Technical Report 14/08, GFZ, Potsdam, doi:10.2312/GFZ.b103-14088. 3

Bergmann-Wolf, I., Forootan, E., Klemann, V., Kusche, J. & Dobslaw, H. (2015). *Updating ESA's Earth System Model for Gravity Mission Simulation Studies: 3. A Realistically Perturbed Non-Tidal Atmosphere and Ocean De-Aliasing Model*, *Tech. rep.*, Scientific Technical Report 14/09, GFZ, Potsdam, doi:10.2312/GFZ.b103-14091. 3

Carrère, L. & Lyard, F. (2003). Modeling the barotropic response of the global ocean to atmospheric wind and pressure forcing - comparisons with observations, *Geophys. Res. Lett.*, **30**, 1997–2000, doi:10.1029/2002GL016473. 15

Dee, D. P. *et al.* (2011). The ERA-Interim reanalysis: configuration and performance of the data assimilation system, *Q. J. Roy. Meteor. Soc.*, **137**, 553–597, doi:10.1002/qj.828. 15

Dobslaw, H., Bergmann-Wolf, I., Dill, R., Forootan, E., Klemann, V., Kusche, J. & Sasgen, I. (2014). *Updating ESA's Earth System Model for Gravity Mission Simulation Studies: 1. Model Description and Validation*, *Tech. rep.*, Scientific Technical Report 14/07, GFZ Potsdam, Potsdam, doi:10.2312/GFZ.b103-14079. 3

Dobslaw, H., Bergmann-Wolf, I., Dill, R., Forootan, E., Klemann, V., Kusche, J. & Sasgen, I. (2015). The updated ESA Earth System Model for future gravity mission simulation studies, *J. Geodesy*, doi:10.1007/s00190-014-0787-8. 10, 15, 55

Dobslaw, H., Flechtner, F., Bergmann-Wolf, I., Dahle, C., Dill, R., Esselborn, S., Sasgen, I. & Thomas, M. (2013). Simulating high-frequency atmosphere-ocean mass variability for dealiasing of satellite gravity observations: AOD1B RL05, *J. Geophys. Res.*, **118**, 3704–3711, doi:10.1002/jgrc.20271. 9, 15

Dobslaw, H. & Thomas, M. (2007). Impact of river run-off on global ocean mass redistribution, *Geophys. J. Int.*, **168**, 527–532, doi:10.1111/j.1365-246X.2006.03247.x. 11

Elsaka, B., Raimondo, J.-C., Brieden, P., Reubelt, T., Kusche, J., Flechtner, F., Iran Pour, S., Sneeuw, N. & Müller, J. (2014). Comparing seven candidate mission configurations for temporal gravity field retrieval through full-scale numerical simulation, *J. Geodesy*, **88**, 31–43, doi:10.1007/s00190-013-0665-9. 9

Flechtner, F. & Dobslaw, H. (2013). *GRACE AOD1B Product Description Document for Product Release 05*, *Tech. rep.*, Rev. 4.0, GRACE Document 327-750, GeoForschungsZentrum Potsdam. 9, 11

Forootan, E., Didova, O., Schumacher, M., Kusche, J. & Elsaka, B. (2014). Comparisons of atmospheric mass variations derived from ECMWF reanalysis and operational fields, over 2003–2011, *J. Geodesy*, **88**, 503–514, doi:10.1007/s00190-014-0696-x. 16

Gruber, T., Bamber, J. L., Bierkens, M. F. P., Dobslaw, H., Murböck, M., Thomas, M., van Beek, L. P. H., van Dam, T., Vermeersen, L. L. A. & Visser, P. N. A. M. (2011). Simulation of the time-variable gravity field by means of coupled geophysical models, *Earth System Sci. Data*, **3**, 19–35, doi:10.5194/essd-3-19-2011. 3, 15

Le Bars, Y., Lyard, F., Jeandel, C. & Dardengo, L. (2010). The AMANDES tidal model for the Amazon estuary and shelf, *Ocean Model.*, **31**, 132–149, doi:10.1016/.ocemod.2009.11.001. 15

Loomis, B. D., Nerem, R. S. & Luthcke, S. B. (2011). Simulation study of a follow-on gravity mission to GRACE, *J. Geodesy*, **86**, 319–335, doi:10.1007/s00190-011-0521-8. 9

Menemenlis, D. & Campin, J.-M. (2008). ECCO2: High resolution global ocean and sea ice data synthesis, *Mercator Ocean Newsletter*, 13–21. 15

Rienecker, M. M. *et al.* (2011). MERRA: NASA's modern-era retrospective analysis for research and applications, *J. Climate*, **24**, 3624–3648, doi:10.1175/JCLI-D-11-00015.1. 15

Saha, S. *et al.* (2010). The NCEP climate forecast system reanalysis, *Bull. Amer. Meteor. Soc.*, **91**, 1015–1057, doi:10.1175/2010BAMS3001.1. 15

Storch, J.-S. V., Eden, C., Fast, I., Haak, H., Hernández-Deckers, D., Maier-Reimer, E., Marotzke, J. & Stammer, D. (2012). An Estimate of the Lorenz Energy Cycle for the World Ocean Based on the STORM/NCEP Simulation, *J. Phys. Oceanogr.*, **42**, 2185–2205, doi:10.1175/JPO-D-12-079.1. 11, 15

Thomas, M., Sündermann, J. & Maier-Reimer, E. (2001). Consideration of ocean tides in an OGCM and impacts on subseasonal to decadal polar motion, *Geophys. Res. Lett.*, **28**, 2457–2460. 11

Visser, P. N. A. M. (2010). Designing Earth Gravity Field Missions for the Future: A Case Study, in: *IAG Commission 2: Gravity, Geoid and Earth Observation, Chania (Greece)*, p. 131–138. 9

Wiese, D. N., Folkner, W. M. & Nerem, R. S. (2009). Alternative mission architectures for a gravity recovery satellite mission, *J. Geodesy*, **83**, 569–581, doi:10.1007/s00190-008-0274-1. 9

Wiese, D. N., Nerem, R. S. & Lemoine, F. G. (2012). Design considerations for a dedicated gravity recovery satellite mission consisting of two pairs of satellites, *J. Geodesy*, **86**, 81–98, doi:10.1007/s00190-011-0493-8. 9

Zenner, L., Bergmann-Wolf, I., Dobslaw, H., Gruber, T., Güntner, A., Wattenbach, M., Esselborn, S. & Dill, R. (2014). Comparison of Daily GRACE Gravity Field and Numerical Water Storage Models for De-aliasing of Satellite Gravimetry Observations, *Surv. Geophys.*, doi:10.1007/s10712-014-9295-x. 9

ISSN 2190-7110